Check for updates

Article

The International Journal of Robotics Research
2021, Vol. 40(8-9) 1015–1044
© The Author(s) 2021
Article reuse guidelines:
sagepub.com/journals-permissions
DOI: 10.1177/02783649211025998
journals.sagepub.com/home/ijr
SAGE

Design of multirotor aerial vehicles: A taxonomy based on input allocation

Mahmoud Hamandi[1], Federico Usai[1], Quentin Sablé[2], Nicolas Staub[1,3], Marco Tognon[1,4] and Antonio Franchi[1,2]

Abstract

This paper reviews the effect of multirotor aerial vehicle designs on their abilities in terms of tasks and system properties. We propose a general taxonomy to characterize and describe multirotor aerial vehicles and their designs, which we apply exhaustively on the vast literature available. Thanks to the systematic characterization of the designs, we exhibit groups of designs having the same abilities in terms of achievable tasks and system properties. In particular, we organize the literature review based on the number of atomic actuation units and we discuss global properties arising from their choice and spatial distribution in the mechanical designs. Finally, we provide a discussion on the common traits of the designs found in the literature and the main open and future problems.

Keywords

Aerial robotics, mechanics, design and control, dynamics

1. Introduction

The study of *unmanned aerial vehicles* (UAVs) has been widely investigated in the last few decades, leading to several well-known applications. In particular, the topic of multirotors has yielded several scientific results in the fields of path planning and control theory, as well as localization and mapping.

These results and their corollary commercial applications are based on a single multirotor design: the *coplanar/collinear propeller design* (with four, six, or eight propellers). In this design, the propeller centers are all placed on the same plane (coplanar) and their angular velocities are collinear, i.e., they produce thrusts all oriented in the same direction. This design is favored for its mechanical simplicity, energy efficiency, and hovering capability, which makes it a good candidate for applications such as visual inspection, survey, and mapping. The system abilities and properties for *coplanar/collinear multirotors* are widely understood in the community, thanks to the vast literature, which comprises well-publicized quadrotors, hexarotors, and octorotors, as well as original designs such as the reconfigurable flying array presented in Oung et al. (2010) and snake-like designs as in Zhao et al. (2017) and Anzai et al. (2017).

In the last decade, several researchers have explored multiple designs of multirotors to overcome some of the limitations of coplanar/collinear designs. Hobby-racers' quest for fast and agile maneuvers led to the exploration of designs allowing more yaw control authority, such as trirotors and Vtail quadrotors. Similarly, works focused on physical interaction and manipulation have led to a large variety of alternative multirotor designs aimed at applying forces and moments to the environments. Design-oriented papers aimed at improving existing designs by adding propellers, increasing thrust-vectoring, or optimizing the propellers' positions and orientations with respect to the main body of the platform to accomplish specific tasks. However, a rigorous classification of such new designs and a comparison of their properties has not yet been addressed in the literature.

This paper aims at presenting an exhaustive and up-to-date review of the vast variety of multirotor designs proposed by the academic and industrial communities in recent years, with an emphasis on the properties and abilities of

[1]LAAS–CNRS, Université de Toulouse, CNRS, Toulouse, France
[2]Robotics and Mechatronics Lab, Faculty of Electrical Engineering, Mathematics and Computer Science, University of Twente, Enschede, The Netherlands
[3]Multi-Robot Systems Group, Faculty of Electrical Engineering, Czech Technical University in Prague, Czech Republic
[4]Autonomous Systems Lab, Department of Mechanical and Process Engineering, ETH Zurich, Zürich, Switzerland

Corresponding author:
Antonio Franchi, University of Twente, Robotics and Mechatronics Lab, Hallenweg 15, 7522 NH Enschede, The Netherlands.
Email: a.franchi@utwente.nl

each platform. The platforms are ordered in classes of designs revolving around the number, nature, and placement of *actuation units*, which are pivotal in defining the motion and interaction capabilities of the platform. In particular, we provide the following.

- A generalized taxonomy that can encompass a large number of multirotor aerial vehicle (MAV) designs. The proposed taxonomy is not based on heuristics and intuitions, but rather on formally derived actuation properties. We also show the relation between such allocation properties and the task abilities of the platforms.
- A complete revision of the majority of MAV designs from the literature, describing them using the above taxonomy. To help the reader, we present each reviewed platform following the increasing number of rotors. In this way, it is natural for the reader to understand what a given platform is capable of. At the same time, the question of which design possesses a given property is provided in an extensive set of summarizing tables across the paper. For a complete understanding of these tables, we provide a summary of all the abbreviations and symbols in Table 1.
- An insight of the manoeuvrability and field of application of each of the mentioned designs.
- A concrete analysis of the feasible force set of each of the reviewed designs.
- Insight on the limitations that we could find in the literature, as well as provide our vision on the directions that should be explored to advance the field of MAV design.

The rest of the paper is organized as follows. Section 2 provides the required definitions to structure the discussion, as well as the modeling of generic multirotor design. Section 3 groups the analysis of different designs based on the number of motors generating thrust. The main findings and generalities that can be extracted from the review are then summarized in Section 4. Finally, conclusions are drawn in Section 5.

Table 1 Summary of the expected entry in each column of the recapitulative tables shown throughout the paper. Note that each table corresponds to platforms with a specific number of atomic actuation units denoted as N.

Entry	Explanation
Apparition	Lists the reference(s) of the paper(s) explaining this design
n_u	Represents the number of actuation controls, including the number of thrusters N in addition to the number of servomotor control inputs
DoFs	Shows which propeller tilt angles are actuated; entries between parenthesis represent angles that are driven synchronously, i.e., constitute one control input
Properties	Lists the possible actuation properties for this design as detailed in Section 2.4
Abilities	Lists the level of all the abilities for this design as detailed in Section 2.6
Maturity	Maturity of the design presented in the apparition paper(s)
Figure	The closest figure representing this design

2. Definitions and conventions

2.1 Review scope

In this paper, we focus our analysis on multirotors, i.e., rotary-wing vehicles, for which the control inputs are solely the spinning velocities of each propeller and, possibly, the propeller orientation. This scope excludes UAV designs where propellers are mixed with wings in which the control input also comprises the wing geometry, i.e., designs in which a subsequent part of the lift is generated by fixed-wing. Some examples are those of Bronz et al. (2017) or the hybrid designs reviewed in Saeed et al. (2015). The scope of this review also excludes multirotors with variable pitch propeller mechanisms, where the propeller pitch is a control input rather than, or in addition to, the propeller speed, e.g., the quadrotor-based design in Michini et al. (2011). Although fixed-speed/variable-pitch propellers provide an alternative for single-input control of thrust, it complicates the ensuing derivation of the platform's dynamics due to the change in relation to the propeller's thrust and drag at a given speed without adding to the taxonomy. Designs in which the motion of weights is used as control input are also excluded, e.g., the quadrotor-based design in Haus et al. (2016). In addition, designs in which the multirotor center of mass (CoM) is time varying are also out of the scope of this paper. This includes some of the previously mentioned cases but also designs where weight motion participates in the system stabilization. Examples of such stabilization systems can be found in Haus et al. (2017), Zhao et al. (2017), and Anzai et al. (2017). Nevertheless, to accommodate for manufacturing imperfections and mechanical constraints, we consider the non-moving CoM in a relaxed way, allowing small displacements of the CoM owing to the motion of the actuators. Lastly, designs where the weight is partially or totally lifted by means other than the rotating propellers are also excluded. This category includes for example platforms lifted through a gas such as helium or ropes, similar to the design presented in Festo AG & Co. KG (2016) and Sarkisov et al. (2019).

Consequently, the considered designs include the control quantities related to: (i) the spinning propellers, each producing mainly a thrust (a lift) and a drag moment; and, possibly, (ii) the vectorization of their orientation in the body frame.

2.2 Design framework

Under the previous assumptions, to describe the various possible designs of small multirotors, we propose a general abstract framework defined as follows.

Definition 1. *A multirotor design is considered as a rigid body, made of fixed mechanical elements, to which some atomic actuation units (AAUs) are attached. The design so defined is completely described by*:

1. *the number of AAUs, denoted by* $N \in \mathbb{N}_{>0}$*;*
2. *the type of every single AAU; and*
3. *the arrangement of the AAUs (position and attitude).*

For the sake of classifying multirotor platforms according to the properties related to their actuation (*actuation properties*), we consider here only the design parameters directly linked to the vehicle actuation. On the other hand, we do not consider design parameters such as total weight, flight electronics, power source, materials, the shape of the structure, and so on. Although very important for the final development of an aerial platform, those parameters are tailored by the particular application and do not grant the platform particular properties of interest for this study.

Remark 1. *In Table 2 we summarize the considered body parts that affect the actuation properties of interest. We shall use these elements as a standard to highlight the main actuation elements and graphically visualize the actuation characteristics of each platform. For each of them, we shall provide a conceptual design representation made of the body parts shown in Table 2.*

We denote by $\mathcal{B}$ the body frame rigidly attached to the multirotor. Its origin O_B coincides with the rigid body CoM and its main axes are denoted by $\boldsymbol{x}_B, \boldsymbol{y}_B, \boldsymbol{z}_B$, respectively.

AAUs. These are the mechatronic components generating thrust. They are the core of each multirotor design. In the literature, they typically consist of a brushless motor with a single propeller.

Considering a generic i th AAU, with $i = 1, \ldots, N$, we denote by $w_i \in \mathbb{R}$ the *propeller rotational speed* and by ${}^{1}\boldsymbol{v}_i \in \mathbb{S}^2$ the coordinates of the *spinning axis* expressed in $\mathcal{B}$.

In addition, we define a frame $\mathcal{F}_{P_i}$ rigidly attached to the i th AAU, with origin O_{P_i} coinciding with its CoM, and with axes $\boldsymbol{x}_{P_i}, \boldsymbol{y}_{P_i}, \boldsymbol{z}_{P_i}$ such that $\boldsymbol{z}_{P_i}$ is the spinning axis ($\boldsymbol{z}_{P_i} = \boldsymbol{v}_i$) and $\boldsymbol{y}_{P_i}$ is perpendicular to both $\boldsymbol{z}_{P_i}$ and ${}^{B}\boldsymbol{p}_i$, where ${}^{B}\boldsymbol{p}_i \in \mathbb{R}^3$ is the position of O_{P_i} with respect to $\mathcal{B}$.

It is convenient to parametrize $\boldsymbol{v}_i$ using two angles α_i and β_i which are defined as follows:

- α_i is the angle needed for a rotation about ${}^{B}\boldsymbol{p}_i$ to bring $\boldsymbol{z}_B$ into a vector $\boldsymbol{z}_{B'}$, where $\boldsymbol{z}_{B'}$ is the projection of $\boldsymbol{z}_B$ into the plane spanned by ${}^{B}\boldsymbol{p}_i$ and $\boldsymbol{z}_{P_i}$;
- β_i is the angle needed for a rotation about the axis perpendicular to the plane spanned by ${}^{B}\boldsymbol{p}_i$ and $\boldsymbol{z}_{P_i}$ to let $\boldsymbol{z}_{B'}$ coincide with $\boldsymbol{z}_{P_i}$.

These two rotations can be combined into a single rotation matrix ${}^{2}{}^{B}\mathbf{R}_{P_i} \in SO(3)$ defined as ${}^{B}\mathbf{R}_{P_i} = \mathbf{R}_2(\beta_i)\mathbf{R}_1(\alpha_i)$ where $\mathbf{R}_1(\alpha_i)$ and $\mathbf{R}_2(\beta_i)$ are the two aforementioned

Table 2 Overview of platform design components: summary of the different components used to design a platform. The different component representations are used hereafter to visualize platform designs.

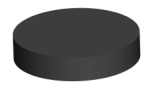	Central body
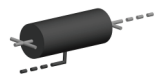	Joint
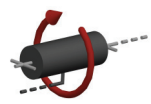	Possibly independently actuated joint
	Counter clockwise (CCW) rotating propeller
	Clockwise (CW) rotating propeller
	Body with a non-tiltable propeller
	Body with a propeller tiltable radially (angle α)
	Body with a propeller tiltable tangentially (angle β)
	Body with a propeller tiltable in $\mathbb{S}^2$ (both angles α and β)
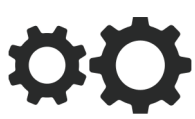	Gears indicating a coupling in the tilting of the corresponding joints

rotations, thus obtaining $\boldsymbol{v}_i = {}^B\boldsymbol{R}_{P_i}\boldsymbol{e}_3$, where $\boldsymbol{e}_3 = [0\ 0\ 1]^{\mathrm{T}}$. Note that such rotations are the ones performed by the two servomotors depicted in Table 2. Furthermore, note that this parametrization is valid as long as ${}^B\boldsymbol{p}_i$ and $\boldsymbol{z}_{P_i}$ are not parallel.

The propeller rotation produces a thrust $\boldsymbol{f}_i \in \mathbb{R}^3$, and a drag moment $\boldsymbol{m}_i \in \mathbb{R}^3$. This force and moment pair applied in O_{P_i} can be expressed with respect to $\mathcal{B}$ as follows:

$$\begin{aligned} \boldsymbol{f}_{P_i} &= c_{f_i}|w_i|w_i\boldsymbol{v}_i \\ \boldsymbol{m}_{P_i} &= k_i c_{\tau_i}|w_i|w_i\boldsymbol{v}_i \end{aligned} \tag{1}$$

where $c_{f_i} \in \mathbb{R}_{>0}$ and $c_{\tau_i} \in \mathbb{R}_{>0}$ are positive constants whose value depends on the shape of the corresponding propeller. The term $k_i \in \{-1, 1\}$ accounts for the direction of rotation of the propeller with respect to $\boldsymbol{v}_i$. As such, $k_i = -1$ (or $k_i = 1$) if the thrust has the same (or the opposite) direction of $\boldsymbol{v}_i$, and the propeller is consequently considered of CCW (or CW) type.

As is normally done in the related literature, in (1) we neglected all the secondary inertia and aerodynamic effects, such as centripetal and flapping effects (see Mahony et al., 2012). In fact, in the considered working conditions, these are negligible with respect to the main thrust and drag moment contributions.

Assuming that the brushless motor can control w_i, we can define $u_{\lambda_i} = |w_i|w_i \in \mathbb{U}_{\lambda_i} \subset \mathbb{R}$ as one of the controllable inputs for the i th AAU. In particular, this is the input that controls the intensity of the produced force and moment. The equations in (1) can be rewritten with respect to $\mathcal{B}$, with the addition of the force-induced moments as follows:

$$\begin{aligned} \boldsymbol{f}_i &= c_{f_i}\boldsymbol{v}_i u_{\lambda_i} \\ \boldsymbol{m}_i &= k_i c_{\tau_i}\boldsymbol{v}_i u_{\lambda_i} + {}^B\boldsymbol{p}_i \times \boldsymbol{f}_i \end{aligned} \tag{2}$$

The parameters required to characterize AAUs are as follows.

1. *Aerodynamic parameters*. The shape of the propeller is an important design factor that defines the lift and drag coefficients, i.e., c_{f_i} and c_{τ_i}, respectively. Those aerodynamic parameters affect the maximum payload and the energy consumption of the vehicle. According to the particular task, the propeller design should be optimized to meet the particular requirements. Although in the above formulation lift and drag coefficients were considered constant, they usually vary throughout their operational range. However, in most applications, propellers are operated in a range where the thrust is constantly proportional to the square of rotational velocity. We make the distinction for bidirectional propellers (propellers rotating in either direction), where the constant coefficients assumption does not hold throughout the propellers' operational range.
2. *Unidirectional or bidirectional thrust.* The second key parameter to consider is the direction of the thrust along the spinning axis. In general, the majority of UAVs in the literature are designed such that the brushless motor controllers rotate the propellers only in one direction, i.e., $0 \leqslant \underline{w}_i \leqslant w_i \bar{w}_i$ where $\underline{w}_i, \bar{w}_i \in \mathbb{R}_{\geq 0}$, making the thrust *unidirectional*. Nevertheless, for some designs with particular brushless motor controllers and propeller profile, as in Brescianini and D'Andrea (2016), the propellers can generate thrust in both directions. In this case $\underline{w}_i \leqslant w_i \leqslant \bar{w}_i$ where $\underline{w}_i \in \mathbb{R}_{<0}$ and $\bar{w}_i \in \mathbb{R}_{>0}$, making the thrust *bidirectional*.

Although this solution enlarges the thrust range, it usually results in a lower thrust magnitude with respect to unidirectional propellers for the same spinning velocity. In fact, it requires propeller designs that are symmetric enough to generate thrust in both directions equally.

3. *Fixed or actuated spinning axis.* The third key parameter to consider for each AAU is its ability to reorient its thrust, either actively or passively. In this case we have that

$$\boldsymbol{v}_i = f_{\boldsymbol{v}_i}(\boldsymbol{u}_{\boldsymbol{V}}) \tag{3}$$

where $f_{\boldsymbol{v}_i} : \mathbb{R}^{n_m} \to \mathbb{S}^2$ and $\boldsymbol{u}_{\boldsymbol{V}} = [u_1 \ldots u_{n_m}]^{\mathrm{T}} \in \mathbb{U}_{\boldsymbol{V}} = \times_{j=1}^{n_m} \mathbb{U}_{\boldsymbol{v}_j} \subset \mathbb{R}^{n_m}$ gathers the angular positions of the shafts of the servo motors that control the orientation of the spinning axis, where we noted by n_m the number of servomotors. Each motor is assumed to be tilted with a maximum of two servomotors, which in turn implies that $n_m \leqslant 2N$. This property can be used to change the vectoring direction of the total thrust produced by the combination of all AAUs without changing their spinning velocities.

In what follows, we consider $\boldsymbol{u}_{\boldsymbol{V}}$ as a state owing to its slower dynamics relative to the applied thrust. Instead, we consider its derivative $\dot{\boldsymbol{u}}_{\boldsymbol{V}}$ as the entity controlled by the n_m servo motors, thus the real input. We can write the dynamic extension of (3):

$$\dot{\boldsymbol{v}}_i = \frac{d\boldsymbol{v}_i}{dt} = \frac{\partial f_{\boldsymbol{v}_i}}{\partial \boldsymbol{u}_{\boldsymbol{V}}}\dot{\boldsymbol{u}}_{\boldsymbol{V}} \tag{4}$$

4. *Position of O_{P_i}.* Finally, the fourth key parameter to consider for each AAU is its position with respect to O_B. In fact, ${}^B\boldsymbol{p}_i$ affects the total moment applied on the CoM of the platform as shown in (2).

Table 3 gathers the previously mentioned parameters and their effects on the produced total thrust and moment. Table 4 summarizes the main abbreviations and notations used in this section and the rest of this paper.

2.3 Platform equations of motion

Let us consider a world frame $\mathcal{W}$, centered in O_W and such that it follows the east–north–up (ENU) convention. Its main axes are denoted by $\boldsymbol{x}_W, \boldsymbol{y}_W, \boldsymbol{z}_W$, respectively.

Table 3 Effect of the AAUs key parameters

AAU key parameter	Short description	Influence
Aerodynamic parameter	Propeller shape	Thrust/drag coefficient
Unidirectional or bidirectional thrust	$\underline{w}_i > 0$ or $\underline{w} < 0$	Thrust and drag direction
Fixed or actuated spinning axis	α fixed or actuated β fixed or actuated	Thrust vectoring
Position of O_{P_i}	${}^B\boldsymbol{p}_i$	Moment generation

Table 4 Summary of the main abbreviations used in the paper and useful mathematical notation

UAV	Unmanned aerial vehicle
AAU	Atomic actuation unit
UDT	Unidirectional thrust
MDT	Multidirectional thrust
FA	Fully actuated
OA	Over actuated
OD	Omnidirectional
$\boldsymbol{F}$	Full allocation matrix
N	Number of AAUs in a platform
n_u	Number of control inputs throughout the paper, it is listed as $n_u = n_\lambda + n_m$
n_λ	Number of thrust input controls
n_m	Number of thrust-vectoring input controls, i.e., number of servo-motors
$\mathbb{U}$	Input control set
$\boldsymbol{v}_i$	Spinning axis of the i th AAU (unit vector)
α_i	Radial tilting angle of the i th propeller
β_i	Tangential tilting angle of the i th propeller
$\mathcal{F}_1$	Image of the feasible force set on the domain $\mathbb{U}$ subject to zero moment

Considering the body frame $\mathcal{B}$ defined previously, its position and orientation with respect to $\mathcal{W}$ are denoted by ${}^W\boldsymbol{p}_B \in \mathbb{R}^3$ and ${}^W\boldsymbol{R}_B \in SO(3)$, respectively. To fully describe the state of the vehicle, we also define the linear velocity of the origin of $\mathcal{B}$ expressed in $\mathcal{W}$ by the vector ${}^B\boldsymbol{\omega}_B \in \mathbb{R}^3$, and the angular velocity of $\mathcal{B}$ with respect to $\mathcal{W}$, expressed in $\mathcal{B}$, by the vector ${}^B_B \in \mathbb{R}^3$.

For the sake of compactness, we introduce the following notation. Let ${}^B\boldsymbol{P}=[{}^B\boldsymbol{p}_1 \cdots {}^B\boldsymbol{p}_N] \in \mathbb{R}^{3\times N}$ and $\boldsymbol{V}=[\boldsymbol{v}_1 \cdots \boldsymbol{v}_N] \in \mathbb{R}^{3\times N}$ be the concatenation matrices of all AAUs positions and spinning axes, respectively. We define the time derivative of $\boldsymbol{V}$ as $\dot{\boldsymbol{V}}=[\dot{\boldsymbol{v}}_1 \ldots \dot{\boldsymbol{v}}_N] \in \mathbb{R}^{3\times N}$. We also denote by $\boldsymbol{u}_\lambda=[u_{\lambda_1} \ldots u_{\lambda_N}]^{\mathrm{T}} \in \mathbb{U}_\lambda \subset \mathbb{R}^{n_\lambda}$ the vector gathering the control inputs relative to the thrust intensity. Note that $\mathbb{U}_\lambda = \times_{i=1}^N \mathbb{U}_{\lambda_i}$, $n_\lambda = N$. The total control input vector is denoted by $\boldsymbol{u}=[\boldsymbol{u}_\lambda^{\mathrm{T}} \boldsymbol{u}_V^{\mathrm{T}}]^{\mathrm{T}} \in \mathbb{U} \subset \mathbb{R}^{n_u}$ and $\mathbb{U}=\mathbb{U}_\lambda \times \mathbb{U}_V$ denotes the set of feasible inputs. Note that, if the orientation of all the AAUs is fixed, i.e., not actuated, then $\boldsymbol{u}=\boldsymbol{u}_\lambda$ and $n_u=n_\lambda$.

Let us define $\boldsymbol{w} \in \mathbb{R}^6$ as the actuation wrench applied to the platform at O_B expressed in $\mathcal{B}$, and $\mathbb{W}$ as the set of feasible wrenches. Following (2), we can write

$$\boldsymbol{w}(\boldsymbol{u}) = \begin{bmatrix} \boldsymbol{f}(\boldsymbol{u}) \\ \boldsymbol{m}(\boldsymbol{u}) \end{bmatrix} = \sum_{i=1}^{N} \begin{bmatrix} \boldsymbol{f}_i(\boldsymbol{u}) \\ \boldsymbol{m}_i(\boldsymbol{u}) \end{bmatrix} \tag{5}$$

Where[3] $\boldsymbol{f} \in \mathbb{R}^3$ and $\boldsymbol{m} \in \mathbb{R}^3$ are the total thrust and moment applied on the platform with respect to $\mathcal{B}$.

To characterize $\boldsymbol{w}$, and in particular how an input variation affects $\boldsymbol{w}$, we introduce the *full allocation matrix* $\boldsymbol{F} \in \mathbb{R}^{6\times n_u}$ defined as

$$\boldsymbol{F}(\boldsymbol{u}) = \frac{\partial \boldsymbol{w}}{\partial \boldsymbol{u}} = \begin{bmatrix} \frac{\partial \boldsymbol{f}}{\partial \boldsymbol{u}_\lambda}(\boldsymbol{u}_V) & \frac{\partial \boldsymbol{f}}{\partial \boldsymbol{u}_V}(\boldsymbol{u}) \\ \frac{\partial \boldsymbol{m}}{\partial \boldsymbol{u}_\lambda}(\boldsymbol{u}_V) & \frac{\partial \boldsymbol{m}}{\partial \boldsymbol{u}_V}(\boldsymbol{u}) \end{bmatrix} = \begin{bmatrix} \boldsymbol{F}_1(\boldsymbol{u}) \\ \boldsymbol{F}_2(\boldsymbol{u}) \end{bmatrix} \tag{6}$$

We decompose $\boldsymbol{F}$ into $\boldsymbol{F}_1 = \partial \boldsymbol{f}/\partial \boldsymbol{u} \in \mathbb{R}^{3\times n_u}$ and $\boldsymbol{F}_2 = \partial \boldsymbol{m}/\partial \boldsymbol{u} \in \mathbb{R}^{3\times n_u}$ referred to as the *force* and *moment allocation matrices*, respectively.

Following the Newton–Euler formalism, we can derive the dynamic equation of a multirotor as follows:

$$\begin{bmatrix} m\,{}^W\ddot{\boldsymbol{p}}_B \\ \boldsymbol{J}^B\dot{\omega}_B \end{bmatrix} = -\begin{bmatrix} mg\boldsymbol{z}_W \\ {}^B\omega_B \times \boldsymbol{J}^B\omega_B \end{bmatrix} + \mathbf{G}\boldsymbol{w}(\boldsymbol{u}) \tag{7}$$

where $m \in \mathbb{R}_{>0}$ and $\boldsymbol{J} \in \mathbb{R}^{3\times 3}_{>0}$ are the total mass and the positive definite inertia matrix with respect to $\mathcal{B}$ of the flying system, g is the gravitational acceleration constant, and $\boldsymbol{G}$ rotates the applied wrench (and, more specifically, $\boldsymbol{f}$) into the world frame for what concerns the translational dynamics, such that

$$\mathbf{G} = \begin{bmatrix} {}^W\boldsymbol{R}_B & \mathbf{0}_{3\times 3} \\ \mathbf{0}_{3\times 3} & \mathbf{I}_{3\times 3} \end{bmatrix} \tag{8}$$

where $\mathbf{I}_{3\times 3}$ is a 3×3 identity matrix.

In the case of a platform where $\dot{\boldsymbol{u}}_V = \mathbf{0}$ (i.e., a platform with fixed propellers, or where the propellers are not actively tilting), thanks to the linearity of $\boldsymbol{w}(\boldsymbol{u})$ with respect to $\boldsymbol{u}_\lambda$, the *full allocation matrix* appears in (7), in particular we have

$$\begin{aligned} \boldsymbol{w}(\boldsymbol{u}) &= \boldsymbol{F}(\boldsymbol{u})[\,\boldsymbol{u}_\lambda \quad \mathbf{0}\,]^{\mathrm{T}} \\ &= \begin{bmatrix} \frac{\partial \boldsymbol{f}}{\partial \boldsymbol{u}_\lambda}(\boldsymbol{u}_V) & \frac{\partial \boldsymbol{f}}{\partial \boldsymbol{u}_V}(\boldsymbol{u}) \\ \frac{\partial \boldsymbol{m}}{\partial \boldsymbol{u}_\lambda}(\boldsymbol{u}_V) & \frac{\partial \boldsymbol{m}}{\partial \boldsymbol{u}_V}(\boldsymbol{u}) \end{bmatrix} \begin{bmatrix} \boldsymbol{u}_\lambda \\ \mathbf{0} \end{bmatrix} \end{aligned} \tag{9}$$

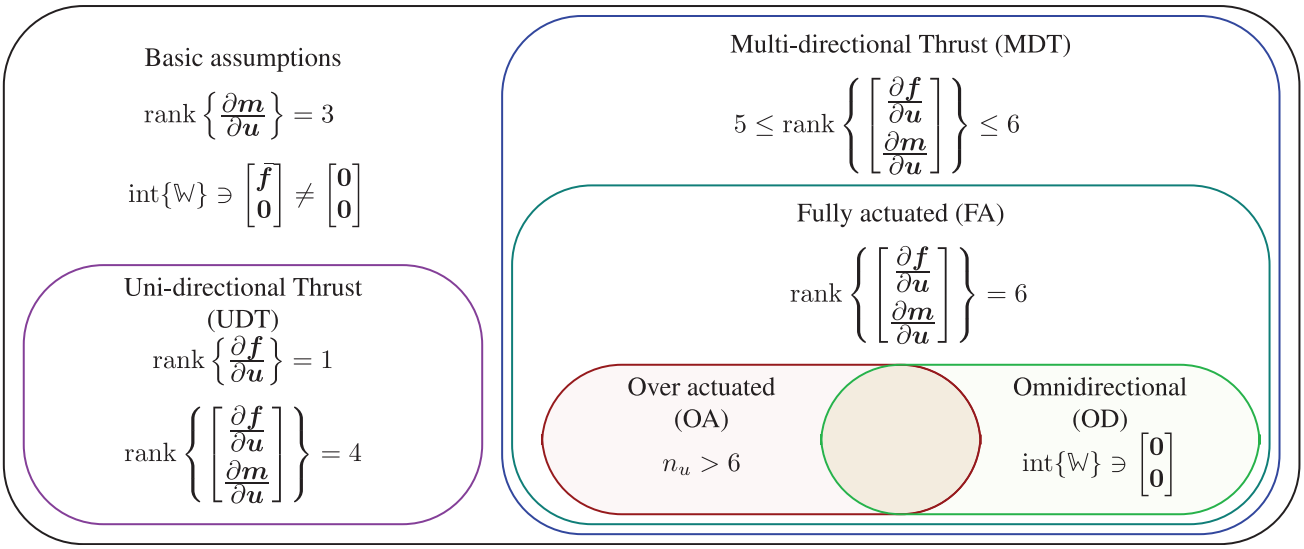

Fig. 1. interaction between thrust related properties for multirotor designs.

As can be seen in (9), in this case the second column of $\boldsymbol{F}(\boldsymbol{u})$ has no effect on the output and will be omitted, for simplicity. Also note that in the case of fixed propellers, the *full allocation matrix* is constant and depends only on $\boldsymbol{u}_V$, which have become constant parameters.

On the other hand, in the case of a platform actively tilting at least one of its propellers, we have to differentiate (7) to make the *full allocation matrix* appear:

$$\begin{bmatrix} m\,{}^W\ddot{p}_B \\ \boldsymbol{J}^B\omega_B \end{bmatrix} = \left({}^W\dot{\boldsymbol{p}}_B, {}^W\boldsymbol{R}_B, \omega_B, {}^B\boldsymbol{P}, \boldsymbol{u}_V\right) + \mathbf{G}\boldsymbol{F}(\boldsymbol{u})\dot{\boldsymbol{u}} \tag{10}$$

where $({}^W\dot{\boldsymbol{p}}_B, {}^W\boldsymbol{R}_B, \omega_B, {}^B\boldsymbol{P}, \boldsymbol{u}_V)$ gathers all the terms that do not depend on the new "virtual" inputs $\dot{\boldsymbol{u}}$ (this technique is known as "dynamic extension"). For the simplicity of notation, from now on, and unless otherwise specified, we omit the dependency of $\mathbf{F}$ on $\boldsymbol{u}$.

Note that the model in (7) and correspondingly in (10) is valid under the following assumptions:

1. motor actuators are controlled by a fast high-gain local controller, to have a negligible transient;
2. gyroscopic and inertial effects due to propellers and motors are considered second-order disturbances that are neglected in the model and can be compensated for by the controller itself, as specified previously;
3. aerodynamic interactions between adjacent propellers are considered negligible, and, again, left to the robustness of the feedback controller;
4. the counter torque on the body produced by a servomotor rotating a propeller is considered negligible and compensated for by the controller.

2.4 System properties

One of the most important characteristics of a design is the set of the admissible wrenches $\mathbb{W}$. In fact, this affects the controllability of the vehicle (how the platform can control its six degrees of freedom (DoFs), e.g., in a coupled or independent way), and the set of reachable states. It is noted that the characterization of $\mathbb{W}$ can be deduced from the number of control inputs n_u, the corresponding subset $\mathbb{U}$, and the *full allocation matrix* $\boldsymbol{F}$. According to the properties of $\boldsymbol{F}$, and more in general of $\mathbb{W}$, we can define the following classes of MAVs which are explained in detail hereafter:

1. unidirectional thrust (UDT);
2. multidirectional thrust (MDT);
3. fully actuated (FA);
4. over-actuated (OA);
5. omnidirectional (OD).

The interactions between the properties of classes (1)–(5) are depicted in Figure 1.

All the listed classes have properties that extend two basic properties holding for any multirotor design and listed in the following.

Property 1. *The total moment can be varied in any direction of* $\mathbb{R}^3$*, i.e.,*

$$\text{rank}\left\{\frac{\partial \boldsymbol{m}}{\partial \boldsymbol{u}}\right\} = 3 \tag{11}$$

This means that for any multirotor design the orientation dynamics is always fully actuated.

Property 2. *Non-zero force and zero moment are an interior-feasible wrench, i.e.,*

$$\text{int}\{\mathbb{W}\} \ni \begin{bmatrix} \bar{\boldsymbol{f}} \\ \mathbf{0} \end{bmatrix} \neq \begin{bmatrix} \mathbf{0} \\ \mathbf{0} \end{bmatrix}. \tag{12}$$

The above two properties are sufficient for the platform to reorient itself in space, and apply a force in at least one direction to counteract its weight without applying any moment (in average), thus remaining in hovering at the equilibrium. These properties are enough for the platform to hover in place, or to move around while being in the near-hovering mode. However, they do not guarantee any decoupling between the moment and the desired force direction. Further properties extend these two and better characterize $\mathbb{W}$, which we recall is computed by mapping $\mathbb{U}$ through the full allocation matrix $\boldsymbol{F}$. Based on the different properties we formally define the following classes.

2.4.1 UDT. This describes platforms for which the total thrust can be varied only along one direction (e.g., in coplanar/collinear designs). This property can be expressed as

$$\text{rank}\left\{\frac{\partial \boldsymbol{f}}{\partial \boldsymbol{u}}\right\} = 1 \quad \text{and} \quad \text{rank}\{\boldsymbol{F}\} = 4, \quad \forall \boldsymbol{u} \in \mathbb{U} \tag{13}$$

2.4.2 MDT. This describes platforms for which the total thrust can be varied along more than one direction independently from the total moment (see, e.g., designs by Kawasaki et al. (2015)) and can be expressed as

$$5 \leqslant \text{rank}\{\boldsymbol{F}\} \leqslant 6, \quad \forall \boldsymbol{u} \in \mathbb{U} \tag{14}$$

2.4.3 FA. This describes a sub-class of MDT platforms, for which the total thrust can be varied along all directions independently from the total moment:

$$\text{rank}\{\boldsymbol{F}\} = 6, \quad \forall \boldsymbol{u} \in \mathbb{U} \tag{15}$$

2.4.4 OA. This term typically describes platforms for which there are more actuation inputs, n_u, than DoFs of the system. In our proposed nomenclature, we limit this definition to only designs which are already FA. This means that a multirotor is OA if the total thrust can be varied along all directions independently from the total moment and with more than one input combination, i.e.,

$$\text{FA} \quad \text{and} \quad n_u > 6 \tag{16}$$

2.4.5 OD. This describes another sub-class of FA designs, not exclusive from OA, where the total thrust can assume any value in a spherical shell independently from the total moment:

$$\text{FA} \quad \text{and} \quad \begin{bmatrix} \bar{\boldsymbol{f}} \\ \mathbf{0} \end{bmatrix} \ni \text{int}\{\mathbb{W}\} \; \forall \bar{\boldsymbol{f}} \in \text{ball}_{\mathbb{R}^3}(R)/\text{ball}_{\mathbb{R}^3}(r) \tag{17}$$

Where[4] $R \geqslant r \geqslant 0 \in \mathbb{R}$, and r, R depend on the limits of the actuators.

The OD property can also be understood from the attainable wrench set $\mathbb{W}$, where the OD sub-class can be represented as follows:

$$\text{FA} \quad \text{and} \quad \begin{bmatrix} \mathbf{0} \\ \mathbf{0} \end{bmatrix} \in \text{int}\{\mathbb{W}\} \tag{18}$$

Remark 2. *The basic properties 1 and 2 guarantee* $[\mathbf{0}^{\mathrm{T}} \; \mathbf{0}^{\mathrm{T}}]^{\mathrm{T}} \in \mathbb{W}$ *for any platform, which can be intuitively applied by setting zero control inputs. However, they do not guarantee that the platform is also OD, because the zero force and moment point may be a boundary point of* $\mathbb{W}$*, i.e., while applying* $\mathbf{0}$ *moment, forces may not be applied in any direction.*

Remark 3. *Tognon and Franchi (2018) conducted a theoretical study to characterize OD multirotors with unidirectional propellers and provide algebraic conditions to reach an OD design in the generic case of* $N \geqslant 7$*. In particular, it has been proved that for a design with unidirectional propellers,* $N = 7$ *is the minimal number of propellers to obtain OD. The authors found similarities between omnidirectional multirotors with unidirectional AAUs, called omniplus* (O_+) *, and frictionless contact grasping (Soto-Guerrero and Ramírez-Torres, 2018).*

Remark 4. *The analysis of such properties is very important for the motion control of the vehicle. In particular, if the platform is FA, then the design of the controller is straightforward. In these cases, the full allocation matrix* $\boldsymbol{F}$ *is full rank and thus invertible. This allows applying simple static (fixed AAUs) or dynamic (orientable AAUs) feedback linearization. In case of fixed AAUs, we can define* $\boldsymbol{u}_\lambda$ *by the inversion of (7) while replacing* $\boldsymbol{w}(\boldsymbol{u})$ *with (9)*:

$$\boldsymbol{u}_\lambda = \boldsymbol{F}^\dagger \mathbf{G}^{-1} \left(\begin{bmatrix} m\,{}^W\ddot{\boldsymbol{p}}_B^\star \\ \boldsymbol{J}^B \dot{\boldsymbol{\omega}}_B^\star \end{bmatrix} + \begin{bmatrix} mgz_W \\ {}^B\boldsymbol{\omega}_B \times \boldsymbol{J}^B \boldsymbol{\omega}_B \end{bmatrix} \right) \tag{19}$$

where ${}^W\ddot{\boldsymbol{p}}_B^\star$ *and* ${}^B\dot{\boldsymbol{\omega}}_B^\star$ *are new virtual control inputs, and* $\boldsymbol{F}^\dagger$ *is the Moore–Penrose inverse of* $\boldsymbol{F}$*. The control law (19) makes the linear and angular accelerations directly controllable.*

In case of orientable AAUs, we can define the dynamic input extension $\dot{\boldsymbol{u}}$ by the inversion of (10):

$$\dot{\boldsymbol{u}} = \boldsymbol{F}^\dagger \mathbf{G}^{-1} \left(\begin{bmatrix} m\,{}^W\dddot{p}_B^\star \\ \boldsymbol{J}^B \ddot{\boldsymbol{\omega}}_B^\star \end{bmatrix} - g \right) \tag{20}$$

where ${}^W\dddot{p}_B^\star$ *and* ${}^B\ddot{\boldsymbol{\omega}}_B^\star$ *are new virtual control inputs. The control law (20) makes the linear and angular jerk directly controllable.*

In both cases, the virtual inputs can be computed with a simple linear state feedback that makes ${}^W\boldsymbol{p}_B^\star$ and ${}^B\ddot{\boldsymbol{\omega}}_B^\star$ stable.

If the platform is also OA, the null space of $\boldsymbol{F}$ can be employed to optimize some appropriate metrics related to the inputs as done, e.g., in Ryll et al. (2015).

On the other hand, if the platform is not FA, feedback linearization cannot be applied directly, and particular attention should be dedicated to the design of the control law. As an example, for the case of a quadrotor, a first input transformation is required in order to consider as input the total thrust and moments. Afterwards, the dynamics need to be differentiated two additional times (up to the snap level) to obtain a full-rank allocation matrix, and apply feedback linearization. Note that, in this case, one needs to consider as a new input the total moment and the second derivative of the total thrust (Mistler et al., 2001).

Although these properties reflect the ability of the platform to apply forces and moments in certain directions and combinations, they do not directly reflect its ability to maneuver, stabilize its position, or interact with its environment. These abilities are affected by the set of feasible control input, $\mathbb{U}$, and on the specific design and hardware extensions added to the platform.

2.5 Feasible wrenches

To assess the reachable allocation capabilities of platform designs, we present throughout the paper a set of representative figures relative to the attainable wrench set $\mathbb{W}$. As this set is a six-dimensional set which is hard to represent in three dimensions, we represent only the three-dimensional projection of the force set while applying zero-moment referred to as $\mathfrak{F}_1$. The choice of the feasible force set with zero-moment is of particular interest for multirotors, e.g., it is important for the static hoverability analysis of the platform (Michieletto et al., 2018).

Remark 5. *The analysis of the feasible force set is calculated in the conditions of (9), where the full allocation matrix is either constant, or assumes the direction of all propellers to be constant, i.e.,* $\dot{\boldsymbol{u}}_{\boldsymbol{V}} = \mathbf{0}$.

For the sake of the representation of $\mathfrak{F}_1$, we detail in the following the analysis of this set for three different cases.

2.5.1 Case 1: Fixed propellers. In the case of fixed propellers, we note that $\boldsymbol{F}$ is constant. Let $\mathbb{U}_2 = null(\boldsymbol{F}_2) \cap \mathbb{U} \subset \mathbb{R}^N$ and $\boldsymbol{B}_2 \in \mathbb{R}^{N \times n}$ be the basis of the null space of $\boldsymbol{F}_2$, where $n = N - rank\{\mathbf{F}_2\}$. We denote by $\Lambda \subset \mathbb{R}^n$ the set $\Lambda = \{\lambda \in \mathbb{R}^n | \boldsymbol{y} = \boldsymbol{B}_2\lambda \in \mathbb{U}\}$, and subsequently

$$\mathbb{U}_2 = \{\boldsymbol{y} \in \mathbb{R}^N | \boldsymbol{y} = \mathbf{B}_2\lambda \ \forall \ \lambda \in \Lambda\} \tag{21}$$

As such, $\mathfrak{F}_1$ can be represented as

$$\mathfrak{F}_1 = \{\boldsymbol{y} \in \mathbb{R}^3 | \boldsymbol{y} = \boldsymbol{F}_1\mathbf{B}_2\lambda \ \forall \ \lambda \in \Lambda\} \tag{22}$$

Owing to the linear relations in (21) and (22), $\mathbb{U}_2$ and $\mathfrak{F}_1$ are convex sets, and it is enough to find the extreme points of Λ to represent the convex hull of $\mathfrak{F}_1$.

The extreme points of Λ are calculated using the algorithm presented in Kleder (2020), where the convex hull of the dual of the polytope (Genov, 2015) defined by $\mathbb{U}_2$ is computed using the results of Barber et al. (1996), from which the convex hull of the polytope $\mathbb{U}_2$ is then computed.

2.5.2 Case 2: Independently tilting propellers. In this case, by a wise change of input coordinates, from $\boldsymbol{u}$ to $\boldsymbol{u}_l$, we can transform the non-linear relation $\boldsymbol{w}(\boldsymbol{u}) = \mathbf{F}(\boldsymbol{V})\boldsymbol{u}$, into a linear one $\boldsymbol{w}(\boldsymbol{u}_l) = \mathbf{F}_l\mathbf{u}_l$. $\mathbf{F}_l$ and $\mathbf{u}_l = [u_{l,1} \ \ldots \ u_{l,n_u}]^{\mathrm{T}}$ are called the augmented allocation matrix and control input, respectively. Note that $\mathbf{F}_l$ does not depend on $\boldsymbol{u}_{\boldsymbol{V}}$.

Considering the representation of $\boldsymbol{v}_i$ by the angles α_i and β_i, the transformation of input coordinates can be described as follows.

1. For a fixed propeller, $u_{l,i}$ corresponds to $u_{\lambda,i}$.
2. For a propeller with only radial tilting, $\mathbf{u}_{l,i} = [u_{\lambda,i}\cos(\alpha_i) \ u_{\lambda,i}\sin(\alpha_i)]^{\mathrm{T}}$.
3. For a propeller with only tangential tilting, $\mathbf{u}_{l,i} = [u_{\lambda,i}\cos(\beta_i) \ u_{\lambda,i}\sin(\beta_i)]^{\mathrm{T}}$.
4. For a propeller tilting in $\mathbb{S}^2$

$$\mathbf{u}_{l,i} = \begin{bmatrix} u_{\lambda,i}\sin(\alpha_i) \\ u_{\lambda,i}\cos(\alpha_i)\cos(\beta_i) \\ u_{\lambda,i}\cos(\alpha_i)\sin(\beta_i) \end{bmatrix} \tag{23}$$

To find $\mathfrak{F}_1$, we define a discrete force search set as follows:

$$\begin{aligned} \mathfrak{F}^d = \{\mathbf{f}^d \in \mathbb{R}^3 | \quad & f_{x,\min} \leqslant f_x^d \leqslant f_{x,\max} \\ & f_{y,\min} \leqslant f_y^d \leqslant f_{y,\max} \\ & f_{z,\min} \leqslant f_z^d \leqslant f_{z,\max}\} \end{aligned} \tag{24}$$

where the range of each force is the expected one given the platform geometry.

Let us consider $\boldsymbol{u}_d$ as the input required to exert a certain force $\boldsymbol{f}_d$ with zero moment, i.e., $\boldsymbol{u}_d = f_l(\boldsymbol{F}_l^{\dagger}[\boldsymbol{f}_d^{\mathrm{T}}, \mathbf{0}_3^{\mathrm{T}}]^{\mathrm{T}})$, where f_l is the map from the augmented control input to the real control input. We then compute $\mathfrak{F}_1$ as the discrete set of forces $\boldsymbol{f}_d \in \mathfrak{F}^d$ whose corresponding required input, $\boldsymbol{u}_d$ is feasible. In details,

$$\mathfrak{F}_1 = \{\mathbf{f}_d \in \mathfrak{F}^d | \mathbf{u}_d = f_l(\mathbf{F}_l^{\dagger}[\mathbf{f}_d^{\mathrm{T}}, \mathbf{0}_3^{\mathrm{T}}]^{\mathrm{T}}) \in \mathbb{U}\} \tag{25}$$

Note that in the case where $n_u > 6$ the pseudo-inverse solution shown above provides one of the infinite solutions to the problem. Owing to the non-linearity in the f_l function, it is not straightforward to find whether an adequate solution exists for a specific $\mathbf{f}_d$ where the pseudo-inverse solution deems the desired force unfeasible. As such, the corresponding $\mathfrak{F}_1$ solution is conservative, while the full solution requires the use of the solution presented below for the jointly tilted propellers.

2.5.3 Case 3: Jointly tilted propellers. We represent $\mathfrak{F}_1$ as the discrete set of forces $\mathbf{f}_d \in \mathfrak{F}^d$, for which the numerical optimization $\|\mathbf{F}(\boldsymbol{u}_V)\mathbf{u}_\lambda - [\mathbf{f}_d^{\mathrm{T}}, \mathbf{0}_3^{\mathrm{T}}]^{\mathrm{T}}\|_2^2$, with the constraint $\mathbf{u} \in \mathbb{U}$ reaches a valid solution. To find such a solution, we employ a gradient-based method such as that presented in Byrd et al. (2000).

2.6 System abilities

The system abilities are expressed with respect to the tasks that can be achieved by the multirotor according to its design. They are all directly related to the attainable wrench set $\mathbb{W}$. We divide these tasks in three representative categories described in the following. These categories encompass the variety of tasks that can be achieved by multirotor systems.

2.6.1 Hovering ability. The ability to hover corresponds to the ability of the platform to remain stationary at the desired position. This represents the main advantage of multirotors over fixed-wing UAVs.

In detail, in the scope of this study, we define *static hovering* as the ability of the platform to stabilize its position and orientation for some ${}^W\boldsymbol{R}_B \in \mathrm{S}O(3)$ with zero linear and angular velocity (i.e., $({}^W\boldsymbol{p}_B, {}^W\boldsymbol{R}_B, {}^W\dot{\boldsymbol{p}}_B, {}^B\boldsymbol{\omega}_B) = ({}^W\boldsymbol{p}_B, {}^W\boldsymbol{R}_B, \mathbf{0}, \mathbf{0})$). This can be achieved (as described by Michieletto et al. (2018)) if at ${}^W\boldsymbol{R}_B$

$$\exists\ \mathbf{u}^* \in \mathbb{U} \text{s.t.} \begin{cases} \boldsymbol{f}(\mathbf{u}^*) & = & mg\boldsymbol{e}_3 \\ \boldsymbol{m}(\mathbf{u}^*) & = & \mathbf{0}_3 \\ \mathrm{rank}\{\boldsymbol{F}\} & \geqslant & 4 \end{cases} \tag{26}$$

Note that in the case of static hovering, it is assumed that the platform can rotate about its $\boldsymbol{z}_B$ axis, i.e., the platform is able to stabilize its orientation about the desired ${}^W\boldsymbol{R}_B$, in addition to any orientation

$$\{\mathbf{Y} | \mathbf{Y} = {}^W\boldsymbol{R}_B \mathbf{R}_{z_B}(\gamma)\ \forall\ 0 \leqslant \gamma \leqslant 2\pi\}$$

Finally, we define *dynamic hovering* (or relaxed hovering) as the ability of the platform to keep the position error bounded while varying its linear and angular velocity. In other words, for these platforms static hovering is not feasible, i.e., $\nexists \mathbf{u}^* \in \mathbb{U}$ s.t. for ${}^W\boldsymbol{R}_B$, $({}^W\dot{\boldsymbol{p}}_B, {}^B\boldsymbol{\omega}_B) = (\mathbf{0}, \mathbf{0})$, however, an approximate hovering is achieved through continuous movement of the platform around a given point.

Following the above definitions, we define the following categories of hovering.

H.0 hovering not possible (e.g., fixed-wing UAVs);
H.1 dynamic hovering (relaxed hovering);
H.2 hovering in a single orientation (e.g., quadrotor, if one disregards rotations about the vertical axis);
H.3 hovering in several orientations (e.g., the TiltHex design presented by Ryll et al. (2017));
H.4 hovering in any orientation (e.g., omnidirectional UAVs).

Categories **H.2**, **H.3**, and **H.4** are subclasses of the family of platforms that can achieve static hovering, with the possible orientations spanning an increasingly large space. We remark that each ability from **H.1** to **H.4** includes the previous abilities.

2.6.2 Trajectory tracking ability. The ability to follow a trajectory is fundamental for many multirotor applications such as surveying, surveillance, and delivery. We propose to categorize the trajectory tracking ability based on the type (position and orientation) and the number of DoFs the multirotor can track independently. While some platforms can trade-off the tracking in position for its orientation counterpart, in our classification we consider positional tracking to have a higher priority than orientation tracking. As such we consider the three-dimensional position tracking ability as a baseline for the tracking ability classifications listed in the following.

TT.1 Only three-dimensional position tracking is possible. Given a desired acceleration in world frame ${}^W\ddot{\boldsymbol{p}}_B$, $\exists \boldsymbol{u}$ s.t. $m{}^W\ddot{\boldsymbol{p}}_B = {}^W\boldsymbol{R}_B\boldsymbol{f}(\boldsymbol{u})$ for a unique choice of ${}^W\boldsymbol{R}_B$.
TT.2 Three-dimensional position and one-dimensional attitude (rotations along a single axis) tracking are possible. Given a desired acceleration in world frame ${}^W\ddot{\boldsymbol{p}}_B$, $\exists \boldsymbol{u}$ s.t. $m{}^W\ddot{\boldsymbol{p}}_B = {}^W\boldsymbol{R}_B\boldsymbol{f}(\boldsymbol{u})$ for any ${}^W\boldsymbol{R}_B$ in a subset of $\mathrm{S}O(3)$ with dimension one (rotations about a single axis).
TT.3 Three-dimensional position and two-dimensional attitude (rotations along two axes) tracking are possible. Given a desired acceleration in world frame ${}^W\ddot{\boldsymbol{p}}_B$, $\exists \boldsymbol{u}$ s.t. $m{}^W\ddot{\boldsymbol{p}}_B = {}^W\boldsymbol{R}_B\boldsymbol{f}(\boldsymbol{u})$ for any ${}^W\boldsymbol{R}_B$ in a subset of $\mathrm{S}O(3)$ with dimension two (rotations about two axes).
TT.4 Three-dimensional position and three-dimensional attitude (rotations along all three axes) tracking are possible. Given a desired acceleration in world frame ${}^W\ddot{\boldsymbol{p}}_B$, $\exists \boldsymbol{u}$ s.t. $m{}^W\ddot{\boldsymbol{p}}_B = {}^W\boldsymbol{R}_B\boldsymbol{f}(\boldsymbol{u})$ for any ${}^W\boldsymbol{R}_B$ in a subset of $\mathrm{S}O(3)$ with dimension three (rotations about three axes).

2.6.3 Physical interaction ability. We also consider the ability to physically interact with the environment, following the rising trend of *aerial physical interaction* (APhI) in the last decade. In particular, we decided to separate the possible APhI abilities according to the following classifications:

APhI.0 APhI not possible;
APhI.1 suitable for tasks such as pushing/pulling;
APhI.2 suitable for carrying a load;
APhI.3 suitable for manipulation tasks.

It should be noted that the APhI abilities require suitable hardware for the specific task, and an adequate level of force and moment decoupling. As explained by Michieletto

et al. (2018), the decoupling between force and moment allows a platform to apply forces in one or more directions while applying null moment. This is a requirement to physically interact with a static environment while maintaining hoverability. It should be noted that the force–moment decoupling of a design can be derived from the study of its full allocation matrix $\boldsymbol{F}$ (Michieletto et al., 2018). It should also be noted that, and to the best of the authors' knowledge, the relation between the allocation matrix and the APhI ability has not been thoroughly studied in the literature, where only the relation between the force–moment decoupling and the APhI ability shown above was presented. However, interesting relations between APhI abilities and the platform's manipulability/maneuverability indexes seems natural and deserve further future study. Accordingly, in what follows each platform is classified based on its demonstrated APhI ability.

2.6.4 Level of maturity. Given the vast literature on multirotor design, we decided to also stress the level of maturity to distinguish purely theoretical contributions from designs that have been constructed and tested in various scenarios. While the theoretical grounding of any design is of paramount importance, we believe that each should be tested by real experiments verifying the corresponding findings. To this goal, we include in our assessment the level of maturity of each design, where the level can be one of the following:

1. theory;
2. simulation of the simplified model (simplistic simulation);
3. simulation with uncertainties and/or second order effects (far from ideal simulation);
4. prototype; and
5. product.

Results deemed as theoretical comprise work where the analysis of the design is conducted without any simulation or prototype. On the other hand, we separate simulation proven designs into two categories, where simplistic simulations that serve as a proof of concept are distinguished from realistic simulations, which include delays, noise, model discrepancies, external perturbations, and so on. The latter reflects a higher degree of maturity of the work and a smaller gap to real experiments. Finally, we label as prototype any work presenting a functional prototype of the proposed design. The final level of maturity would describe designs implemented as commercial products, but we note that such occurrences are rare.

3. Unirotor (one AAU)

Even though the case of a multirotor composed of a single AAU is a contradiction in itself, it is considered for completeness of the review; in addition, it can represent a configuration reached in the case of extreme failure of multirotors. To the best of the authors' knowledge, the only occurrence of such design fitting this paper scope (i.e., excluding moving mass and control surface) can be found in Zhang et al. (2016).

Table 5 Recapitulative table for $N = 1$

Apparition	Properties	Abilities	Maturity
Zhang et al. (2016)	None	H.1, TT.1, APhI.0	Prototype

The proposed approach relies on active control and demonstrates a position tracking controller for such a vehicle. Due to its single rotor $n_u = 1$, the vehicle is under constant rotation, however, the prototype was shown to be able to achieve relaxed hovering. The system assessment is listed in Table 5.

4. Birotor (two AAUs)

Birotors are composed of only two AAUs as their name suggests (Table 6). For these designs, hovering can only be achieved if thrust vectoring is controlled, i.e., the total thrust is dynamically oriented during flight. The two AAUs are always rotating in opposing directions to have a zero total drag moment when the propellers spin at the same speed, thus the platform can hover without being subjected to constant rotation. In addition, in most designs, the multirotor CoM is placed between the two AAUs to benefit from a damped pendulum dynamics, such as in the work of Chowdhury et al. (2012), where a wing-tail was also added for stabilization as shown in Figure 2.

4.1 Tilting in $\mathbb{S}^2$ Designs

The fist pioneering work on birotor design was presented by Gress (2002), in which the inertia and gyroscopic characteristics of the multirotor are exploited to control the roll, pitch, and yaw in order to achieve a stable hover. The two AAUs are devised to be tilting in $\mathbb{S}^2$ independently, thus $n_u = 2 + 4$ as shown in Figure 2. Further studies were conducted by Kendoul et al. (2006) and Amiri et al. (2011), providing the dynamic model of such designs and introducing some refinements to increase controllability. In the latter, the two AAUs generate unidirectional thrust actuated independently in $\mathbb{S}^2$. As the resulting dynamic model is highly non-linear and hard to exploit for control purposes, a simplified model was introduced by Kendoul et al. (2006) which allows considering backstepping approaches for control.

Another platform presenting propellers tilting in $\mathbb{S}^2$ was proposed by Sanchez et al. (2008), where the authors considered the same design as in Gress (2002) (Figure 2) while enforcing both AAUs to have the same tilting angles, leading to $n_u = 2 + 2$. This design reduces the computational

Table 6 Recapitulative table for the birotors ($N = 2$)

Apparition	n_u	DoFs	Properties	Abilities	Maturity	Figure
Gress (2002) Kendoul et al. (2006) Amiri et al. (2011)	$2+4$	$\alpha_1, \alpha_2, \beta_1, \beta_2$	FA	H.3, TT.2, APhI.0	Prototype	Figure 2
Sanchez et al. (2008)	$2+2$	$(\alpha_1, \alpha_2)\ (\beta_1, \beta_2)$	UDT	H.2, TT.2, APhI.0	Prototype	Figure 2
Donadel et al. (2014)	$2+2$	β_1, β_2	UDT	H.2, TT.2, APhI.0	Realistic simulation	Figure 2
Prothin and Moschetta (2013)	$2+4$	$\alpha_1, \alpha_2, \beta_1, \beta_2$	FA	H.3, TT.2, APhI.0	Prototype	Figure 3
Papachristos et al. (2011)	$2+2$	α_1, α_2	UDT	H.2, TT.2, APhI.0	Prototype	Figure 2
Chowdhury et al. (2012)	$2+2$	α_1, α_2	UDT	H.2, TT.2, APhI.0	Simplistic simulation	Figure 2
Blouin and Lanteigne (2014)	$2+2$	α_1, α_2	UDT	H.2, TT.2, APhI.0	Prototype	Figure 2
Cardoso et al. (2016)	$2+2$	α_1, α_2	UDT	H.2, TT.2, APhI.0	Realistic simulation	Figure 2

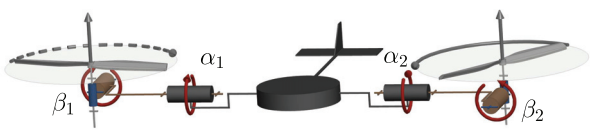

Fig. 2. Conceptual 3D kinematic representation of a generic birotor design with wing-tail stabilization.

complexity of the control while still being able to achieve hovering in the conducted experiments.

Prothin and Moschetta (2013) presented another design, named the "donut," made of two AAUs aligned vertically with the center of the multirotor frame, which can be tilted independently in $\mathbb{S}^2$ as shown in Figure 3, thus obtaining again $n_u = 2+4$. The details of the dynamical model are presented and the authors propose to leverage the tilting to use drift force and moment as control inputs.

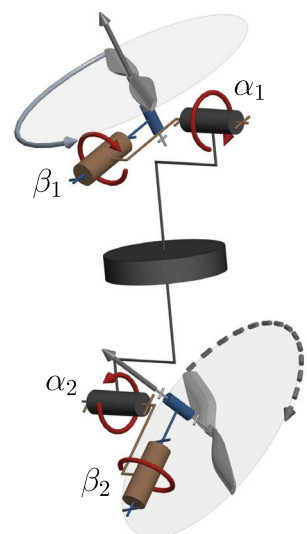

Fig. 3. Conceptual three-dimensional kinematic representation of the birotor design presented in Prothin and Moschetta (2013)

4.2 Radial and tangential tilting designs

A birotor design often found in the literature is presented in Papachristos et al. (2011), where the platform has two AAUs placed on an axis above the CoM of the platform, and tilting independently radially about their axis, thus resulting in $n_u = 2+2$. This design provides the option to tilt almost perpendicularly to the vertical direction, and thus the platform can generate most of its lift laterally to redirect its lift in the desired flight direction. In this design, yaw is achieved by tilting propellers about opposite α angles, roll is achieved by applying different thrust in each propeller, and pitch is achieved by tilting both propellers equally in the direction of the desired pitch, where the pitching moment is relative to the tilting angle and the vertical distance between the propellers' CoM and the platform CoM. This design is illustrated in Figure 2.

A similar design was presented by Chowdhury et al. (2012), where the authors proposed a controller that changes the tilt angles to achieve desired roll and yaw independently and demonstrated their controller in simulation. Another similar controller was proposed by Blouin and Lanteigne (2014), however, they tested their controller on a prototype. Finally, Cardoso et al. (2016) presented a robust controller for this platform design and showed its path-tracking ability in a realistic simulation under external disturbances and model uncertainties.

Donadel et al. (2014) proposed a design where the tangential tiltings are fixed and the two radial tiltings are actuated, hence, again, $n_u = 2+2$, with propellers' CoM also above the CoM of the platform as shown in Figure 2. They proposed a control approach relying on optimal H_∞/H_2 techniques, which they validated in realistic simulations.

5. Trirotor (three AAUs)

Trirotors are composed of three AAUs. As such, they can be considered as an upgrade from birotors, but they pose a challenge due to the unbalanced moment caused by the odd

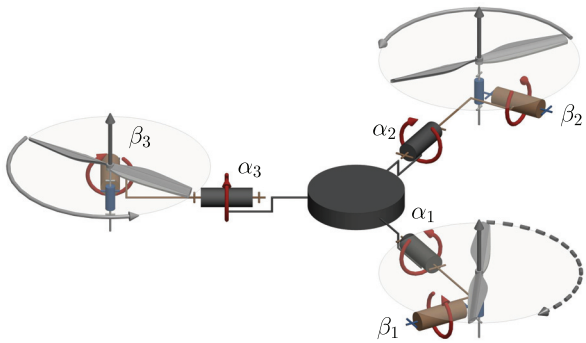

Fig. 4. Conceptual three-dimensional kinematic representation of a generic trirotor Δ-configuration design.

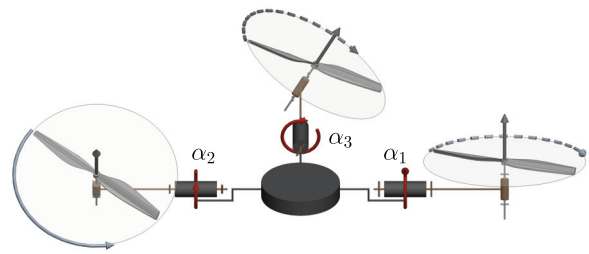

Fig. 5. Conceptual three-dimensional kinematic representation of a generic trirotor T-configuration design. The tail propeller (typically smaller and weaker) is depicted on the top while the frontal principal propellers (typically larger and stronger) are on the bottom. The sagittal axis points down in the picture.

number of propellers. In addition, and similarly to birotors, the low number of actuators imposes limitations on the achievable performance, in particular in the ability to perform stable hovering (Kataoka et al., 2011).

One of the first trirotor designs appeared in Rongier et al. (2005), where propellers are tilted at a fixed angle so that a non-collinear thrust is ensured. The control is based on a combination of aircraft gyroscopic effect with a piezo-sensor to detect the tilt angle (pitch and roll) with respect to the horizontal orientation. However, the lack of control of the yaw angle forces the rotor to constantly rotate about its CoM, thus being unable to achieve the basic static hovering ability (**H.2**). The design is demonstrated on a prototype powered with a cable and shown in Figure 4; as the platform constantly rotates, it stretches the cable causing a failure of the proposed controller.

Multiple designs have been later proposed in the literature that aim to balance the odd shape of the trirotor, which we group into *T-configurations* and Δ *-configurations*. In addition, to overcome the limitation of the number of actuators, which are not enough to achieve the basic **H.2**, several works have proposed to add one or more additional actuators in order to achieve thrust-vectoring, thus making the platform able to gain the **H.2** ability.

5.1 T-configuration

This setup is composed by two frontal *principal propellers*, that may be dynamically tilted or fixed, spinning in opposite directions, with a third propeller (typically smaller) mounted on a *tail* as shown in Figure 5. This one, in general, tilts around the radial axis in order to improve pitch and yaw control.

5.1.1 Tail-only tilting propeller. This design was presented in Salazar-Cruz and Lozano (2005), followed by Salazar-Cruz et al. (2009). The *tail-propeller* is endowed with a servo motor which allows the control of the yaw motion by tilting about the sagittal axis, and the pitch angle regulating the propeller rotational speed. The two main frontal fixed

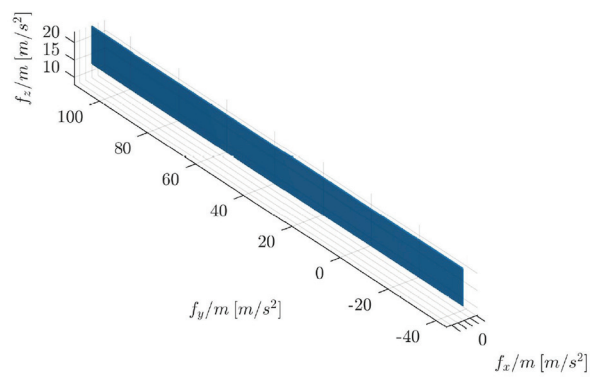

Fig. 6. Visualization of the $\mathfrak{F}_1$ set of the design presented in Salazar-Cruz et al. (2009) normalized by the platform mass. T-shaped trirotor with tail tilting radially and with two fixed main propellers. Here $N = 3$ and $n_u = 3 + 1$. Profile description: two-dimensional plane perpendicular to the tail rotation plane.

propellers are in charge of the control of total thrust and roll angle. In total, we have $n_u = 3 + 1$. The $\mathfrak{F}_1$ set is represented in Figure 6.

In the mentioned works, the hovering and the forward flight control of this vehicle were achieved using a nonlinear controller based on nested saturations. The same design is instead controlled in Yoon et al. (2013) with an optimal linear–quadratic regulator (LQR) to control the attitude. All these works have been validated with an experimental prototype.

5.1.2 Frontal-propeller tilting. In a design presented in Papachristos and Tzes (2013) and Papachristos et al. (2014, 2016), the two frontal principal propellers are also able to tilt radially with the same (locked) tilting angle, while the tail rotor can tilt independently, thus obtaining $n_u = 3 + 2$. This approach was adopted to allow the vehicle to apply a push-force (APhI.1) in the sagittal direction. To improve the control scheme and platform stability, in Papachristos et al. (2016) a model predictive control (MPC) approach was implemented.

Table 7 Recapitulative table for the trirotors ($N = 3$)

Apparition	n_u	DoFs	Properties	Abilities	Maturity	Figure
Rongier et al. (2005)	3			H.1, TT.1, APhI.0	Prototype	Figure 4
Salazar-Cruz and Lozano (2005)	$3+1$	α_3	UDT	H.2, TT.2, APhI.0	Prototype	Figure 5
Salazar-Cruz et al. (2009)						
Yoon et al. (2013)						
Papachristos and Tzes (2013)	$3+2$	$(\alpha_1, \alpha_2), \alpha_3$	MDT	H.2, TT.2, APhI.1	Prototype	Figure 5
Papachristos et al. (2014)						
Papachristos et al. (2016)						
Cerberus RC Tilt-Rotor	$3+2$	α_1, α_2	MDT	H.3, TT.3, APhI.0	Product	Figure 5
Escareno et al. (2008)	$3+1$	$(\alpha_1,\alpha_2,\alpha_3)$	UDT	H.2, TT.2, APhI.0	Prototype	Figure 4
Mohamed and Lanzon (2012)	$3+3$	$\alpha_1,\alpha_2,\alpha_3$	FA	H.3, TT.4, APhI.0	Simplistic simulation	Figure 4
Kastelan et al. (2015)	$3+3$	$\alpha_1,\alpha_2,\alpha_3$	FA	H.3, TT.4, APhI.0	Prototype	Figure 4
Servais et al. (2015b)	$3+3$	$\alpha_1,\alpha_2,\alpha_3$	FA	H.3, TT.4, APhI.0	Prototype	Figure 4
Servais et al. (2015a)						
Ramp and Papadopoulos (2015)	$3+6$	$\alpha_1,\alpha_2,\alpha_3, \beta_1,\beta_2,\beta_3$	OA	H.3, TT.4, APhI.0	Realistic simulation	Figure 4

A commercially available T-configuration trirotor is the *Cerberus Tilt-Rotor*.[5] In this product the two frontal principal propellers can tilt radially independently, while the tail propeller is fixed, thus obtaining again $n_u = 3+2$. However, its kinematics is different from the previous one. The $\mathfrak{F}_1$ set of the Cerberus Tilt-Rotor is similar to the $\mathfrak{F}_1$ set represented in Figure 6.

5.2 Δ-configuration

This design is composed of three propellers of the same dimension arranged on a triangle, with two of them spinning in opposite directions. In addition, in these configurations the thrust is roughly shared equally by all three motors, encouraging the symmetrical placement of the motors on a circle (i.e., every $2\pi/3$) as shown in Figure 4.

One example design was presented in Escareno et al. (2008), where the authors built a Δ-configuration multirotor with all propellers being allowed to tilt radially with the same angle, thus obtaining $n_u = 3+1$. While the propellers' tilting is used to directly control the yaw motion, its effect on pitch and roll behavior is compensated for as a disturbance. The overall control system is robust with respect to dynamic couplings, in particular gyroscopic effects, and shows a maneuverability similar to that of a quadrotor but with a more compact design as well as a longer autonomy, thanks to the lower number of motors.

Another Δ-configuration design was presented in Mohamed and Lanzon (2012), where each propeller can be tilted independently in its radial direction in a range of $[-\pi/2, \pi/2]$, thus obtaining $n_u = 3+3$. The resulting is a fully actuated vehicle, controlled with H_∞ loop shaping, and achieving full-pose tracking. Similar designs were studied in Kastelan et al. (2015) and Servais et al. (2015a,b), and the $\mathfrak{F}_1$ set of such designs is represented in Figure 7.

On the other hand, Ramp and Papadopoulos (2015) presented an over-actuated system, where each of the three propellers is allowed to rotate independently in both its tangential and radial direction, thus obtaining $n_u = 3+6$. This over-actuated system was tested in a realistic simulation, where it proved its ability to achieve full-pose tracking, and we provide its $\mathfrak{F}_1$ set in Figure 8. To find the desired thrust and orientations, the controller is designed to find the desired force vector for each propeller independently, which is then achieved by reorienting the propeller to the desired direction and applying the desired thrust.

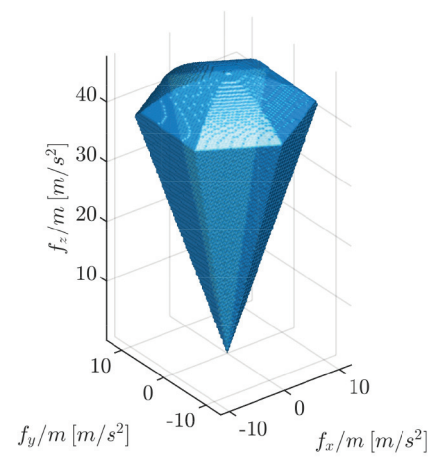

Fig. 7. visualization of the $\mathfrak{F}_1$ set of a Δ-trirotor normalized by the platform mass, where the platform has independent radial tilting of all three propellers; tilting angle limits are chosen at $\pm 30^\circ$. Here $N = 3$ and $n_u = 6$. Profile description: hexagonal pyramid with the tip at zero enclosed with a dome.

Table 7 summarizes all the presented designs.

6. Quadrotor (four AAUs)

This case is of particular interest because for designs with fixed AAUs, $N = 4$ is the minimum number of propellers necessary to achieve the basic actuation assumptions summarized in (11) and (12), in addition to the UDT property and the static hovering ability **H.2**.

Table 8 Recapitulative table for the quadrotors ($N = 4$)

Apparition	n_u	DoFs	Properties	Abilities	Maturity	Figure
Mahony et al. (2012) Bouabdallah et al. (2004) Bouabdallah and Siegwart (2005)	4		UDT	H.2, TT.2, APhI.2	Product	
Falanga et al. (2017)	4		UDT	H.2, TT.2, APhI.0	Prototype	Figure 11
Ryll et al. (2012) Ryll et al. (2013) Ryll et al. (2015)	$4+4$	$\alpha_1,\alpha_2,\alpha_3,\alpha_4$	OA/OD	H.3, TT.4, APhI.0	Prototype	Figure 11
Falconi and Melchiorri (2012)	$4+4$	$\alpha_1,\alpha_2,\alpha_3,\alpha_4$	OA	H.3, TT.4, APhI.0	Simplistic simulation	Figure 11
Oosedo et al. (2016)	$4+4$	$\alpha_1,\alpha_2,\alpha_3,\alpha_4$	OA	H.3, TT.4, APhI.0	Prototype	Figure 11
Yih (2016)	$4+4$	$\alpha_1,\alpha_2,\alpha_3,\alpha_4$	OA	H.3, TT.4, APhI.0	Realistic simulation	Figure 11
Nemati and Kumar (2014) Nemati et al. (2016)	$4+2$	$(\alpha_1,\alpha_3),(\alpha_2,\alpha_4)$	FA	H.3, TT.4, APhI.0	Prototype	Figure 11
Badr et al. (2016)	$4+4$	$\beta_1,\beta_2,\beta_3,\beta_4$	FA	H.3, TT.4, APhI.0	Simplistic simulation	Figure 13
Devlin et al. (2018)	$4+4$	$\beta_1,\beta_2,\beta_3,\beta_4$	OA	H.3 TT.4 APhI.1	Prototype	Figure 13
Scholz et al. (2016)	$4+2$	$(\beta_1,\beta_2),(\beta_3,\beta_4)$	FA	H.3, TT.4, APhI.0	Simplistic simulation	Figure 13
Long et al. (2012)	$4+4$	β_1,β_2,β_3	FA	H.3,TT.4, APhI.0	Prototype	Figure 14
Long et al. (2014)	7	β_1,β_2,β_3				
Senkul and Altug (2013)	$1+8$	$\alpha_1,\alpha_2,\alpha_3,\alpha_4,\beta_1,\beta_2,\beta_3,\beta_4$	UDT	H.2, TT.2, APhI.0	Simplistic simulation	Figure 15
Senkul and Altug (2014)	$4+8$	$\alpha_1,\alpha_2,\alpha_3,\alpha_4,\beta_1,\beta_2,\beta_3,\beta_4$	OA	H.2, TT.2, APhI.0	Simplistic simulation	Figure 15
Hua et al. (2015) Odelga et al. (2016)	$4+2$	$(\alpha_1,\alpha_2,\alpha_3,\alpha_4),(\beta_1,\beta_2,\beta_3,\beta_4)$	FA	H.4, TT.4, APhI.0	Simplistic simulation	Figure 16
De Martini et al. (2017)	$4(\mathrm{B}i)+2$	$(\alpha_1,\alpha_2,\beta_1,\beta_2),(\alpha_3,\alpha_4,\beta_3,\beta_4)$	FA	H.4, TT.4, APhI.0	Simplistic simulation	Figure 15
Khoo et al. (2017)	$4+8$	$\alpha_1,\alpha_2,\alpha_3,\alpha_4,\beta_1,\beta_2,\beta_3,\beta_4$	OA	H.3, TT.4, APhI.0	Prototype	Figure 15
Segui-Gasco et al. (2014)	$4+8$	$\alpha_1,\alpha_2,\alpha_3,\alpha_4,\beta_1,\beta_2,\beta_3,\beta_4$	OA	H.3,TT.4, APhI.0	Prototype	Figure 15
Kawasaki et al. (2015)	$4+2$	$(\alpha_1,\alpha_3,\beta_1,\beta_3),(\alpha_2,\alpha_4,\beta_2,\beta_4)$	MDT	H.3, TT.3, APhI.1	Prototype	Figure 17
McArthur et al. (2017)	$4+1$	α_1	MDT	H.2, TT.2, APhI.1	Prototype (partiallytested)	Figure 18

The first documented quadrotor design in the literature traces back to 1907 and documented in Young (1982). While this design recorded a few tethered flights, the modern quadrotor design (Pounds et al., 2002) traces its origin back to the same platform concept, however, technological advancements within the last century has allowed new platforms to be built with compact electronics and sensors, allowing robust and agile maneuvers.

While the first designs relied on a coplanar/collinear propeller configuration, later modifications were conducted to extend the system properties via thrust-vectoring. All the presented designs consider the AAUs and the CoM to be located roughly on the same plane. We refer to Table 8 as a summary of the presented designs.

6.1 Coplanar/collinear designs

For modeling, control, and the general theory of classical coplanar/collinear designs one can refer to Mahony et al. (2012), Bouabdallah et al. (2004) and Bouabdallah and Siegwart (2005), and Pounds et al. (2010), which are three comprehensive references among the vast literature of such designs. We present an example of $\mathfrak{F}_1$ set of such designs in Figure 9. Note that the designs with less than four AAUs cannot obtain such nice mono-dimensional shape (UDT ability) because they need at least a tilting rotor to achieve the static hovering ability (H.2). This makes the coplanar/collinear quadrotor the simplest platform of its kind, i.e., with a minimum number of total inputs (servo and brushless motors) that has a decoupled force and moment spaces.

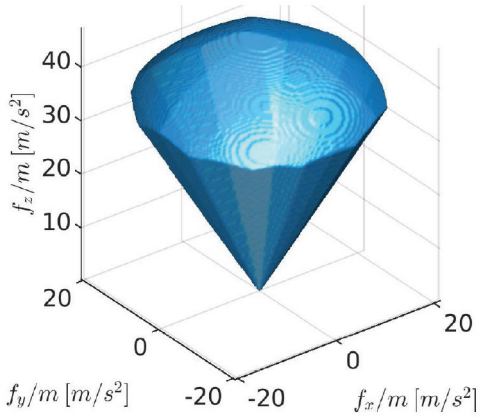

Fig. 8. visualization of the $\mathfrak{F}_1$ set of the design presented in Ramp and Papadopoulos (2015) normalized by the platform mass. The design consists of a Δ-trirotor with all propellers independently tilting both radially and tangentially; tilting angle limits are chosen at $\pm 30^{\circ}$. Here $N=3$ and $n_u=9$. Profile description: dodecagonal pyramid with the tip at zero with top enclosed with a dome.

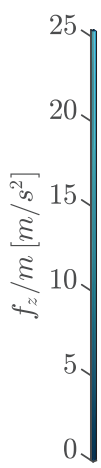

Fig. 9. Visualization of the $\mathfrak{F}_1$ set of a fixed coplanar/collinear quadrotor design normalized by the platform mass. Here $N=4$ and $n_u=4$. Profile description: line along the CoM of the platform.

Such decoupling significantly simplifies the control problem and is one of the reasons for the success of quadrotors.

Note that the wide attention gathered by coplanar/collinear quadrotors comes from the combination they offer between their simple mechanics and relative easiness of control for trajectory tracking, thanks to the dynamic feedback linearizability (or, equivalently, the differential flatness) of the non-linear system dynamics (Mistler et al., 2001).

This enabled a vast set of applications for coplanar/collinear designs. Innovative modular designs such as that presented in Zhao et al. (2017), exhibit the same properties as classical coplanar/collinear designs, although they lie

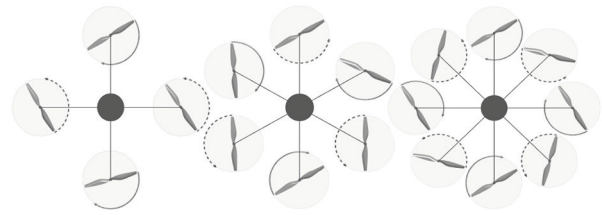

Fig. 10. Top view of the conceptual kinematic representation of coplanar designs with (left to right) four, six, and eight propellers.

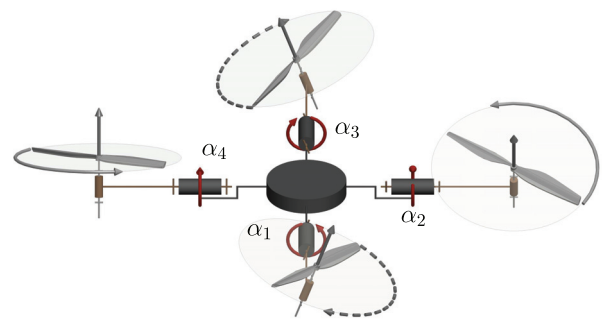

Fig. 11. Conceptual 3D kinematic representation of a generic quadrotor with propellers tilting/tilted about their radial axes.

outside the scope of this paper due to their varying CoM with each new configuration.

In addition, coplanar/collinear designs for $N>4$, shown in Figure 10, (typically $N=6$ or $N=8$) will not be discussed hereafter as their properties are the same as the $N=4$ case. Their coplanar/collinear distribution leads to similar results for all such designs despite the increase of the control inputs. The only notable differences are: (i) the increase of the control authority due to the increase of AAUs, which translates mostly in an increase of payload; and (ii) the possible redundancy, i.e., AAUs failure can be mitigated while preserving the design's properties.

6.2 Radial tilting designs

Some designs consider AAUs which are radially tilted/tilting in order to achieve total thrust vectoring for quadrotors as shown in Figure 11. Within the other two tilting directions, this particular design can be considered as the simplest mechanical extension to the coplanar/collinear design achieving thrust vectoring.

Falanga et al. (2017) presented a quadrotor with propellers tilted 15° radially about their relative axes, i.e., $n_u=4$. The tilt angle is computed to increase yaw control, and was tested on a prototype flying through a narrow gap. Figure 11 most closely resembles the described design, however, with the propellers' tilt being constant.

Ryll et al. (2012) proposed a configuration, further analyzed in Ryll et al. (2013, 2015), where four additional servomotors are used to independently radially tilt the AAUs,

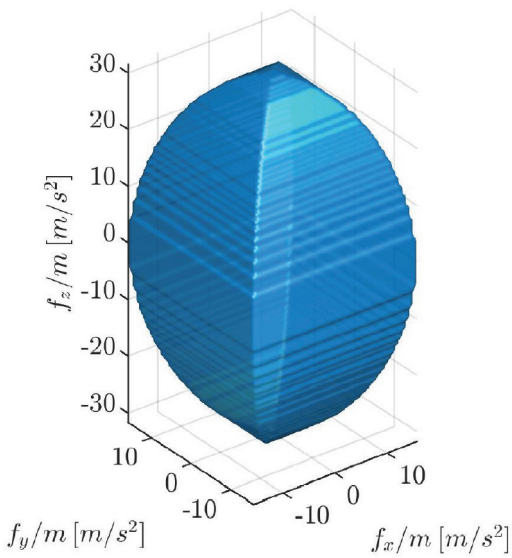

Fig. 12. Visualization of the $\mathfrak{F}_1$ set of the design presented in Ryll et al. (2012) normalized by the platform mass. The design consists of a quadrotor with all propellers independently tilting about their corresponding radial axis. Here $N = 4$ and $n_u = 8$.

thus obtaining $n_u = 4 + 4$, resulting in an over-actuated system, with the corresponding $\mathfrak{F}_1$ set presented in Figure 12. By considering the servo dynamics and the aerodynamic effects, the authors derived and proposed a highly coupled system, which proves difficult to manage from a control point of view. To mitigate these shortcomings, the classical approach neglects the servo-motor dynamics and assumes the employment of high-gain controllers which can achieve instantaneous tracking. In addition, the aerodynamic effects are modeled in the controller as external disturbances. These simplifications allow the use of feedback linearization techniques with dynamic extension, for a desired trajectory tracking of class $\mathcal{C}^3$. The system over-actuation is dealt with a pseudo-inverse allocation, that is used to obtain a minimum energy thrust generation. The design and corresponding controller have been validated through simulation and experimental implementation.

Falconi and Melchiorri (2012) considered a similar design with the implementation of an inverse dynamic controller, to compensate for the non-linear dynamics, and a PD with feedforward to impose a position and attitude trajectory. Similarly to Ryll et al. (2015), Falconi and Melchiorri (2012) solved the allocation problem using a pseudo-inverse approach. This approach is more sensitive to model uncertainty due to the complexity of the aerodynamic modeling.

Oosedo et al. (2016) studied a wide range of platform orientations in addition to the transition from horizontal to vertical hovering of the multirotor. Position and orientation are regulated through a PID loop while control allocation techniques for two orientation sets are proposed and validated experimentally.

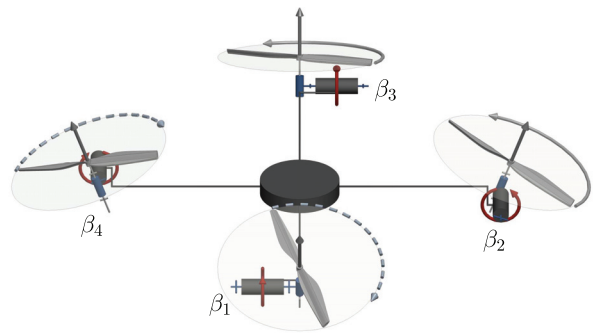

Fig. 13. Conceptual three-dimensional kinematic representation of a generic quadrotor with propellers tilting/tilted about their tangential axes.

Yih (2016) authors considered the same design subjected to model uncertainties. They proposed a robust sliding mode controller for position and orientation tracking, augmented with a chattering suppression block to improve its performance. The proposed model and control law were validated in simulation.

Nemati and Kumar (2014) considered similar radial tilting of the AAUs while constraining paired AAUs to tilt the same angle in opposing directions, thus obtaining $n_u = 4 + 2$. This results in a fully actuated system (non-over-actuated). A trajectory tracking goal has been achieved by PD regulators. Nemati et al. (2016) built and tested the described design.

6.3 Tangential tilting designs

Another attempt at extending the classical quadrotor design is to consider tangential tilting of the AAUs, see Figure 13, as in Badr et al. (2016), which has also $n_u = 4 + 4$. To maintain the moment balanced, the AAUs rotation direction is non-standard. Indeed usually CW and CCW AAUs are alternating along the four summits of their square distribution, but in this proposed design they are grouped two by two. This choice allows to have more control authority for pitch and roll motions while decoupling roll from the y-translation and pitch from the x-translation. Badr et al. (2016) developed a controller that resorts in simplifying assumptions based on the trajectory characteristics. This control is tested for a simple trajectory in simulation to validate the decoupling between rotational and translational dynamics. A similar design to the latter was presented by Devlin et al. (2018), with each propeller rotating independently in the tangential direction, thus obtaining again $n_u = 4 + 4$. The platform is named *ElbowQuad*. The design was tested via a real experiment on a prototype of the design.

Scholz et al. (2016) also studied the design shown in Figure 13. To control the platform they synchronized the rotational speed of each of the four AAUs, then derived an input allocation scheme based on heuristics and proposed a

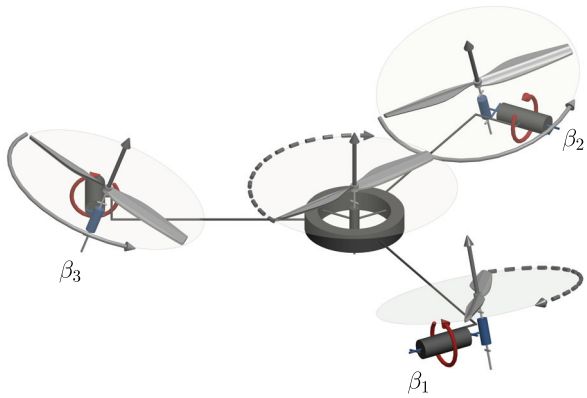

Fig. 14. Conceptual three-dimensional kinematic representation of the quadrotor design presented in Long et al. (2014, 2012). The three non-central propellers are tilting about their tangential axes independently.

backstepping approach. The controller tracks the desired orientation, altitude, and velocity in the plane, and is robust to unmodeled dynamics. The authors rely on optimization techniques to tune the controller gains. This approach is corroborated with simulation comprising sensor noise.

Another design with tangential tilting of the AAUs can be found in Long et al. (2012), with $n_u = 4 + 4$, and Long et al. (2014), with $n_u = 4 + 3$, named *Omnicopter*. The latter is shown in Figure 14. In this proposed design one main AAU (with either one or two propellers sharing the same axis of rotation with opposed rotation directions) is significantly bigger than the other propellers and is placed in the center of the platform with its thrust direction aligned with the z_B axis of the body frame. The other three AAUs, smaller in size, are distributed around the main one in a triangular distribution and allowed to tilt tangentially.

Long et al. (2012)used a backstepping approach and a PID loop to achieve decoupled tracking of both orientation and position. The control allocation is achieved by considering a linearization of the system around the functioning point. Long et al. (2014) proposed the same design with only one central AAU to improve the efficiency of the design. They apply the same control technique for the second design and validate both designs via real experimentations on a prototype.

6.4 Tilting in $\mathbb{S}^2$ designs

The following designs explore the AAUs tilting in $\mathbb{S}^2$ as illustrated in Figure 15, in order to achieve thrust vectoring in all directions for each AAU. Note that due to the mechanical complexity involved in such a design, most of the presented work considering non-fixed AAUs are only studied theoretically.

The first original design can be found in Şenkul and Altuğ (2013, 2014), where the authors considered a classical quadrotor with each AAU being able to tilt both radially and tangentially. Şenkul and Altuğ (2013) considered all

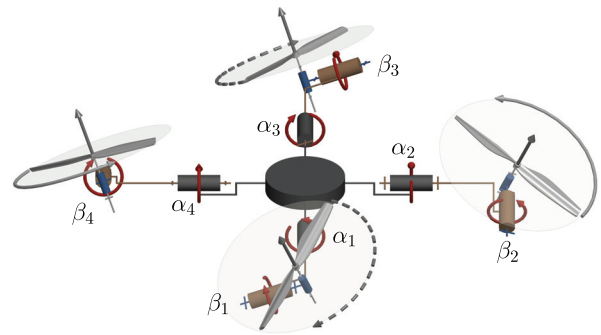

Fig. 15. Conceptual three-dimensional kinematic representation of a generic quadrotor with propellers tilting/tilted in $\mathbb{S}^2$, i.e., about both the radial and tangential axes.

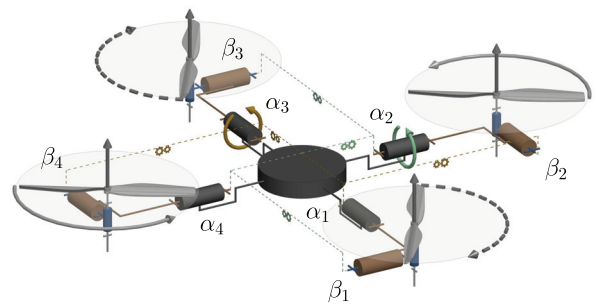

Fig. 16. Conceptual three-dimensional kinematic representation of a quadrotor with propellers tilting/tilted in $\mathbb{S}^2$ presented in Hua et al. (2015) and Odelga et al. (2016). The locked tilting that makes all the propellers point always in the same direction is highlighted.

AAUs to tilt independently while rotating at the same speed, hence $n_u = 1 + 8$. Then the full potential of this design is exploited in Şenkul and Altuğ (2014), where the authors allow independent tilting of the propellers, $n_u = 4 + 8$. The authors propose a cascaded PID control loop with adaptive gains to account for the gyroscopic effect arising from the propellers. The above two approaches are validated with simple simulations to show their trajectory tracking ability.

Similarly to Şenkul and Altuğ (2013), Hua et al. (2015) proposed to study a quadrotor tilting in $\mathbb{S}^2$ as shown in Figure 16, and such that the total thrust vectoring is achieved by tilting each AAU equally in the same thrust direction. This scheme allows the platform to apply unidirectional thrust but in a direction that is tiltable in $\mathbb{S}^2$ thus obtaining $n_u = 4 + 2$. The authors proposed a control scheme that primarily tracks a reference position or velocity (similar to a coplanar/collinear quadrotor with fixed propellers), then rotates the thrust direction to point in the desired orientation. Position and orientation are proved to be decoupled, which is validated in a simple trajectory tracking simulation.

The same design as shown in Figure 16 was explored in Odelga et al. (2016), with the addition of an explicit

mechanism design that enforces the angles to rotate equally, whereas in Hua et al. (2015) it was only theoretically assumed. Full-actuation allows the use of a standard feedback linearization control with dynamic extension, which is validated by simulation. The introduction of a real mechanism makes explicit the constraints induced by the mechanism limits. Therefore, tracking performances are limited by unidirectional rotors and tilt angle limits, despite the full actuation nature of the design.

De Martini et al. (2017) also presented a quadrotor design with propellers tilting synchronously in $\mathbb{S}^2$ as shown in Figure 15. The synchronization allows the vehicle to fly across a narrow passage, where each pair of propellers is assumed to be tilting about a given axis, with $n_u = 4 + 2$. Furthermore, bidirectional AAUs are considered and physical mechanism constraints are neglected. The proposed control scheme is based on PID and model inversion and validated in a simple simulation. The multirotor orientation is computed in order to allow the navigation through a narrow passage geometry.

The above contributions have presented analyses and simulations studying quadrotors with propellers tilting in $\mathbb{S}^2$. In what follows, we introduce the contributions that presented a working mechanical system with propellers either tilting in $\mathbb{S}^2$, or tilted about a fixed orientation throughout their flight.

Khoo et al. (2017) implemented a design as shown in Figure 15 that allows independent rotation of all propellers, thus obtaining $n_u = 4 + 8$. The prototype is controlled with a multi-surface sliding mode controller, followed by a pseudo-inverse control allocation.

Segui-Gasco et al. (2014) also built a prototype, while considering tilting limits of each AAU in its control. The dynamics of the system are derived while considering the gyroscopic moment produced by the fast tilting AAUs. The authors consider a coplanar/collinear quadrotor controller, with body orientation and total thrust calculated through system linearization and weighted pseudo-inverse. The over-actuation of the system calls for control allocation, which is calculated in an energy-optimal way. The authors validated their approach with a hovering maiden flight, and their design analysis suggested the need for high inertia propellers to increase the produced torque and allow higher vehicle speeds.

Another design with the AAUs tilting in $\mathbb{S}^2$ can be found in Kawasaki et al. (2015), where the authors proposed a design such that the AAUs are tilted independently by pairs as shown in Figure 17, where we can see that each pair of propellers are connected to a single axis actuated with a servomotor that can induce an equivalent tilt in both α and β to both propellers, i.e., $n_u = 4 + 2$. The authors proposed a control scheme for trajectory tracking which takes into account the effect of the AAUs' airflow interference. The performance of the platform is demonstrated with a prototype while sliding along a surface.

McArthur et al. (2017) presented a quadrotor design based on the composition of a Δ-trirotor (see Section 5) with an additional tail propeller tangentially tilted to provide thrust in a lateral direction as shown in Figure 18. The design is endowed with this extra propeller to help push an object. All propellers in this design are fixed, except for the trirotor tail which is actively tilted radially, $n_u = 4 + 1$. The proposed design was implemented in a prototype used to validate the extra push abilities in a planar experiment (APhI.1) without flying; in this experiment, the coplanar/collinear propellers were turned off, and an extra propeller was added to control the yaw just during these experiments.

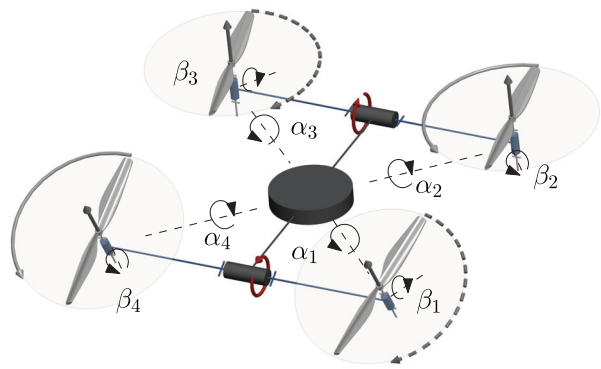

Fig. 17. Conceptual three-dimensional kinematic representation of a quadrotor with propellers tilting in $\mathbb{S}^2$ as presented in Kawasaki et al. (2015).

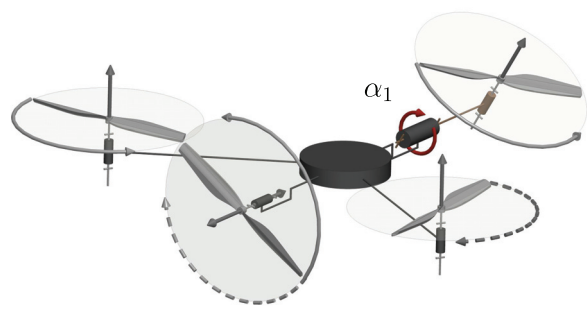

Fig. 18. Conceptual three-dimensional kinematic representation of a quadrotor with propellers tilting/tilted radially/tangentially as presented in McArthur et al. (2017).

While the quadrotor design was exploited extensively in the literature and allowed platforms to reach OA/OD, the limited number of propellers does not allow the platforms to exhibit more than UDT and **H.2** without any servomotors. While quadrotors are still very popular, many papers from the literature exploit designs with $N>4$ to exploit actuation properties higher than UDT, especially for applications of APhI, where lateral forces are often required.

7. Pentarotor (five AAUs)

The case of $N = 5$ AAUs is not commonly found in the literature, owing to its lack of symmetry implied by the odd number of AAUs. Usually, symmetric designs are favored thanks to their ease of control and diagonal inertia matrix.

Table 9 Recapitulative table for the pentarotors ($N = 5$)

Apparition	n_u	Properties	Abilities	Maturity	Figure
Albers et al. (2010)	5	MDT	H.3, TT.3, APhI.1	Prototype	Figure 19

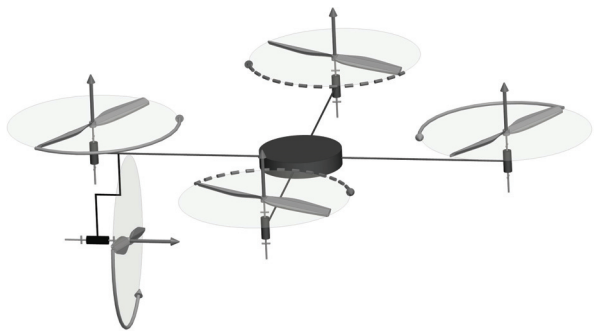

Fig. 19. Conceptual three-dimensional kinematic representation of the pentarotor design presented in Albers et al. (2010).

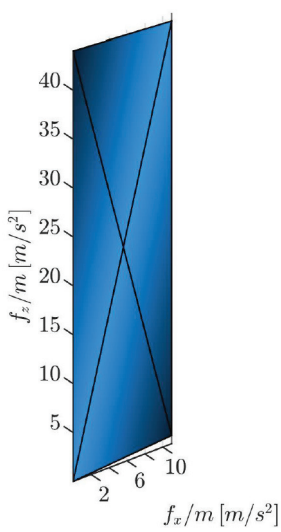

Fig. 20. Visualization of the $\mathfrak{F}_1$ set of the design presented in Albers et al. (2010) normalized by the platform mass. The design consists of a quadrotor with an additional propeller pointing in a lateral direction. All propellers are fixed. Here $N = 5$ and $n_u = 5$. Profile: subsurface of the xz-plane, where we assume the fifth propeller is pointing in the x-direction. The surface has the largest height for $x = 0$ and decreases as x increases.

The only documented non-coplanar/collinear pentarotor design we could find is introduced in Albers et al. (2010) and can be described as a classical coplanar quadrotor with the addition of a propeller oriented in an orthogonal direction to provide extra actuation for attaining the considered tasks; a conceptual design sketch is shown in Figure 19, and the design properties and abilities are listed in Table 9. The goal is to be able to easily apply a normal force on a wall for tasks such as inspection, cleaning, and painting.

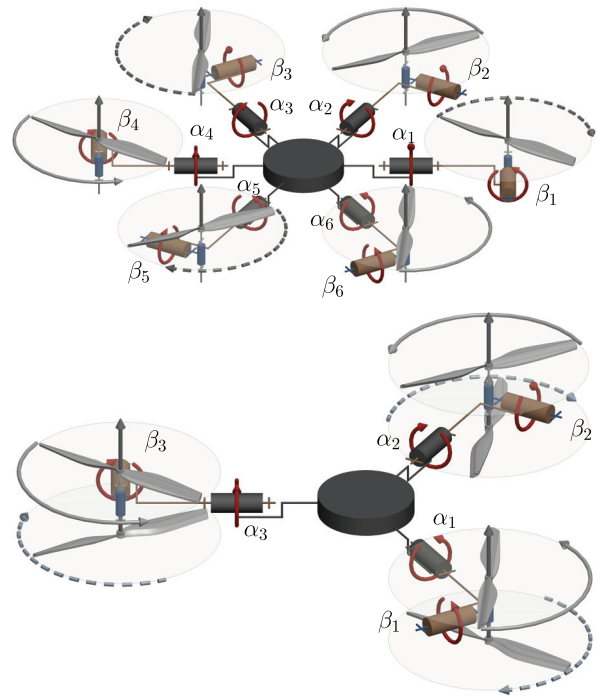

Fig. 21. Conceptual three-dimensional kinematic representation of (top) star-shaped hexarotor and (bottom) Y-shaped hexarotor with propellers tilting/tilted in $\mathbb{S}^2$.

All the AAUs' orientations are fixed, thus $n_u = 5$. Owing to its composition design, it holds the same properties as a classical coplanar quadrotor, plus the ability to push along one extra translational direction. The proposed design was tested on a prototype, and its $\mathfrak{F}_1$ set is presented in Figure 20.

8. Hexarotor (six AAUs)

A hexarotor design has $N = 6$. For hexarotors, we can group coplanar/collinear designs into two groups, star-shaped and Y-shaped as shown in Figure 21 top and bottom, respectively. The former refers to a distribution where each AAU is a vertex of the star, while the latter considers a disposition similar to the delta trirotor. The system properties and capabilities are the same as for the coplanar/collinear quadrotor, except that the Y-shaped hexarotor is robust to AAU failure, whereas the star-shaped hexarotor is not (see Michieletto et al., 2017).

As for hexarotors with tilted AAUs, tilting angles can be chosen so that $\boldsymbol{F}$ is full-rank, and thus the platform is fully actuated. In fact, this is the minimal configuration for

Table 10 Recapitulative table for the hexarotors ($N = 6$)

Apparition	n_u	DoFs	Properties	Abilities	Maturity	Figure
Jiang and Voyles (2014)	6		FA	H.3, TT.4, APhl.0	Prototype	Figure 21(top)
Ryll et al. (2016)	$6+1$	$(\alpha_1,\alpha_2,\alpha_3,\alpha_4,\alpha_5,\alpha_6)$	FA	H.3, TT.4, APhl.0	Realistic simulation	Figure 23
Bicego (2019)					Prototype	
Kamel et al. (2018)	$6+6$	$\alpha_1,\alpha_2,\alpha_3,\alpha_4,\alpha_5,\alpha_6$	OD	H.4, TT.4, APhl.0	Prototype	Figure 25
Elkhatib (2017)						
Giribet et al. (2016)	6		FA	H.3, TT.4, APhl.0	Realistic simulation	Figure 21(top)
Pose et al. (2017)						
Soto-Guerrero and Ramírez-Torres (2018)	$6+6$	$\beta_1,\beta_2,\beta_3,\beta_4,\beta_5,\beta_6$	OA	H.3, TT.4, APhl.1	Simplistic simulation	Figure 21(top)
Crowther et al. (2011)	$6+1$	$(\alpha_1, \alpha_2, \alpha_5, \alpha_6, \beta_1, \beta_2, \beta_5, \beta_6)$	OA	H.3, TT.4, APhl.0	Prototype	Figure 21(top)
Ryll et al. (2017)	6		FA	H.3, TT.4, APhl.1	Prototype	Figure 21(top)
Staub et al. (2018)	6		FA	H.3, TT.4, APhl.3	Prototype	Figure 21(top)
Rajappa et al. (2015)	6		FA	H.3, TT.4, APhl.0	Simplistic simulation	Figure 21(top)
Morbidi et al. (2018)	$6+2$	$(\alpha_1, \alpha_2, \alpha_3, \alpha_4, \alpha_5, \alpha_6), (\beta_1, \beta_2, \beta_3, \beta_4, \beta_5, \beta_6)$	OA	H.3, TT.4, APhl.0	Simplistic simulation	Figure 23
Rashad et al. (2017)	6(Bi)		OD	H.4, TT.4, APhl.0	Realistic simulation	Figure 21(top)
Rashad et al. (2019)	6		FA	H.3, TT.4, APhl.1	Prototype	Figure 21(top)
Myeong et al. (2019)	$6+1$	$(\alpha_1, \alpha_2, \beta_1, \beta_2)$	OA	H.3, TT.4, APhl.1	Prototype	Figure 21(bottom)

which it is possible to obtain FA of the six-dimensional pose without any dynamic tilting of the propellers. However, as the AAUs are tilted, part of the energy is dissipated internally to balance the platform while hovering; as such, tilt-angles have to be chosen as a trade-off between propulsive efficiency (i.e., closer to coplanar/collinear) and maneuverability in the sense of decoupling between actuation force and moment. This choice can be made either based on heuristics or by optimizing a cost function specific to the application at hand. The impact of both radial and tangential tilting, in the case of unidirectional fixed-tilt AAUs for hexarotor, is formally studied in Michieletto et al., 2017. It appears that a sufficient condition to ensure full-rankness of $\boldsymbol{F}$ is to have non-null tangential tilting even in the absence of radial tilting. However, if the tangential tilting is small enough, $\boldsymbol{F}$ is close to loose full-rankness, i.e., has a large condition number, and if the tilting is too important internal forces augment and the design loses energy efficiency. To alleviate that effect, radial tilting can be introduced as a way to lower the condition number for small tangential tilting. It is also proven that hexarotors, for which AAUs are only radially tilted, are *fully vulnerable* to AAU failure.

As most of the hexarotor designs found in the literature consider unidirectional fixed-tilt AAUs, thus obtaining $n_u = 6$, in what follows AAUs are assumed to have a fixed-tilt unless specified otherwise. Table 10 summarizes the properties and abilities of the hexarotor designs reviewed in the following.

8.1 Radial tilting designs

In Jiang and Voyles (2014) (and previous work) the design focused on allowing *force closure*, i.e., the ability to instantaneously resist six-dimensional wrench perturbation such as wind while in contact with the environment. To obtain such a design, AAUs are radially tilted by a constant angle of 20°, obtained considering a manipulability index (Yoshikawa, 1985); the design is tested on a prototype. The $\mathfrak{F}_1$ set of similar designs is shown in Figure 22.

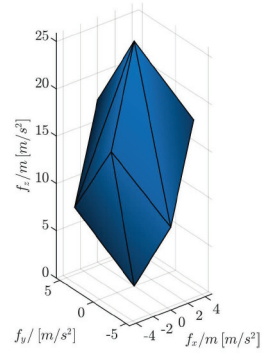

Fig. 22. Visualization of the $\mathfrak{F}_1$ set of a hexarotor with propellers equally tilted about a fixed α angle, the $\mathfrak{F}_1$ set is normalized by the platform mass. Here $N = 6$ and $n_u = 6$. Profile description: trigonal trapezohedron.

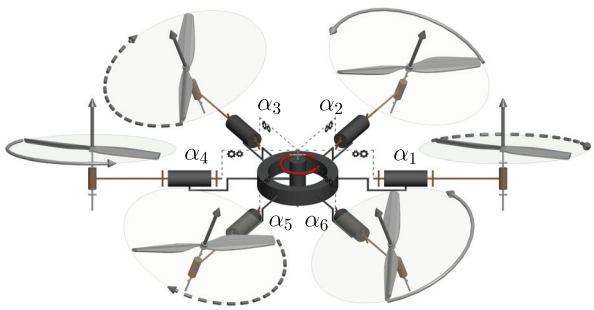

Fig. 23. Conceptual three-dimensional kinematic representation of the *FastHex* design presented in Ryll et al. (2016). The propellers are tilting radially. Highlighted the locked tilting that forces all the propellers to tilt of the same angle α.

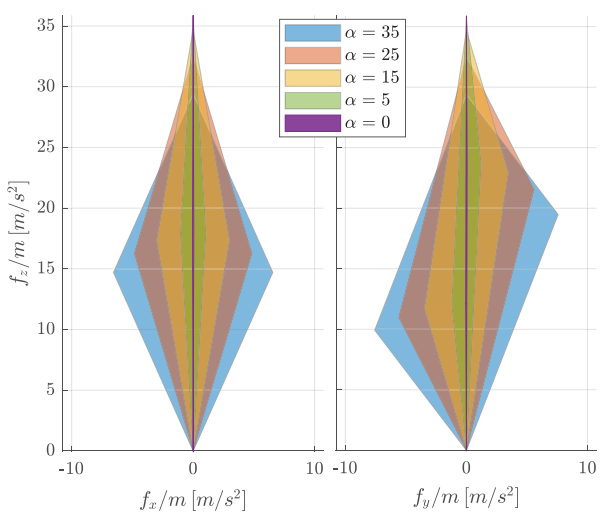

Fig. 24. Visualization of the $\mathfrak{F}_1$ set of the *FastHex* design at different propeller tilts α intersection with (right) $x = 0$ plane and (left) $y = 0$ plane. The $\mathfrak{F}_1$ set is similar to coplanar/collinear design for $\alpha = 0$; as α increases, the platform is capable of applying further lateral forces while decreasing the possible lift.

On the other hand, Ryll et al. (2016) presented a design called *FastHex* where AAUs' radial tilting can be changed simultaneously with a single servomotor for all AAUs as shown in Figure 23, thus obtaining $n_u = 6 + 1$. This allows switching between UDT and FA configurations of the multirotor with only one additional input. This design can be used to optimize between energy efficiency during free-flight (coplanar/collinear AAUs) and an adequate force/moment decoupling during physical interactions. Figure 24 illustrates the different possible $\mathfrak{F}_1$ sets at different tilts. Extensive simulations validate the benefits of such a design for a real case scenario, whereas later Bicego (2019) also validated these results in real-world experiments.

In Kamel et al. (2018) and Elkhatib (2017), each AAU is equipped with a servomotor (six in total) to tilt independently, thus obtaining $n_u = 6 + 6$. The design, named *Voliro*, was tested on a prototype showing successful omnidirectional flights and is shown in Figure 25.

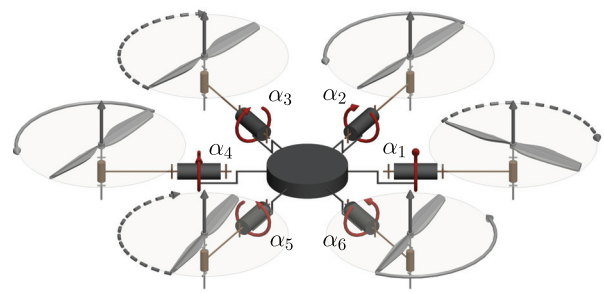

Fig. 25. Conceptual three-dimensional kinematic representation of the *Voliro* design presented in Kamel et al. (2018) and Elkhatib (2017). The propellers are tilting radially and all independently.

8.2 Tangential tilting designs

Differently from the designs in Section 8.1, Giribet et al. (2016) proposed a design where the AAUs are tangentially tilted, at a magnitude chosen heuristically at $\beta = 13^\circ$. The authors have demonstrated the ability of a vehicle with small tilting to be able to face failure in one of its propellers. Trajectory tracking of the platform was validated through simulation with noise and rotor failure.

Pose et al. (2017) also proposed a design relying on tangentially tilted AAUs, where the tilting angle is heuristically chosen in a range that ensures the robustness of the design to failures, at a fixed $\beta = 17^\circ$ for all AAUs. The controller does not exploit the MDT property of the design and focuses on emulating the behavior of coplanar design, by only considering a reduced output vector and finding optimal control allocation to the spinning velocity of the most solicited AAU. This design is shown to be robust to single AAU failure through experiments on a prototype of the design.

The above two designs are mechanically equivalent despite the different choice of tilt angle β, however, the controlled output of each is different, with Pose et al. (2017) not fully exploiting the FA property.

Another design is proposed in Soto-Guerrero and Ramírez-Torres (2018), where the authors combined a hexarotor with a hexapod design, mounting each propeller on one of the platform's legs, which can rotate about two axes corresponding to the propeller's arrangement about the CoM, and the propeller's tangential tilt. The platform is able to crawl and fly, and hence its name *hexapodopter*. The authors prove that their design can achieve FA, and assess their design through simulation.

8.3 $\mathbb{S}^2$ tilting designs

Crowther et al. (2011) presented a hexarotor design where each AAU is allowed to tilt in $\mathbb{S}^2$. Crowther et al. (2011) described designs constrained such that the thrusts produced by each pair of AAUs are aligned along three orthogonal directions, possible AAUs' orientations and direction are further grouped into three classes. The authors

validated their feedback linearization-based controller in a static experiment on a prototype of one of the detailed classes. This enforced orthogonality ensures that each six-dimensional translation is actuated by a single AAU which comes at the logical corollary cost that each AAU should be able to sustain the full weight of the design. The authors also compared their design with a coplanar design which maximizes propulsive efficiency

Conversely, the following works considered the tilting of the AAUs in a more general way, i.e., not enforcing orthogonality of the individual thrusts. In addition, we note that most works considering generic AAUs orientation in $\mathbb{S}^2$, are interested in finding the optimal AAUs orientations and thus consider both radial and tangential tilting in their optimization problem formulation, even if the resultant optimal orientation does not always comprise both tiltings.

Another design was proposed in Mehmood et al. (2016), where the tilt angles about $\mathbb{S}^2$ are chosen to optimize maneuverability, defined as the maximum acceleration reached in a given direction. The paper also investigates the failure of a single propeller and concludes with theoretical contributions.

Tadokoro et al. (2017) investigated an optimal design based on "dynamic manipulability measure." It can be understood as omnidirectional acceleration capabilities similar to the manipulator case and is expressed as $\sqrt{\det \boldsymbol{F}\boldsymbol{F}^{\mathrm{T}}}$. This work also proves that it is sufficient to study the planar disposition of the AAUs, as any spatial distribution can be brought to its equivalent plane form (neglecting some mass/inertia changes, and not taking aerodynamic cross-wind into account).

Both methods rely on heavy symmetry constraints imposed on the design, in terms of AAU disposition and tilting. Interestingly, the optimal design for these two metrics does not require AAUs to be oriented in $\mathbb{S}^2$, only radial tilting of around 37° and 35° for Mehmood et al. (2016) and Tadokoro et al. (2017), respectively. However, we do note that only radial tilting renders the design *fully vulnerable* to AAU failure (Michieletto et al., 2017).

The aforementioned maxima are also acknowledged in Rajappa et al. (2015), where the AAU tiltings are adjusted before flight such as to minimize the norm of the control effort upon the desired trajectory. Indeed, it is important to underline that the optimal value of the tilt angles is highly dependent on the specific trajectory that the UAV has to perform. The problem has been solved searching for an optimal arrangement with respect to a minimum control effort over a desired trajectory. In the end, a feedback linearization technique has also been exploited.

Ryll et al. (2017) described a design to enable physical interaction. AAUs are tilted symmetrically to guarantee a trade-off between maximum lateral forces and losses due to internal forces, the magnitude of the tilting angles are 30° and 10°, respectively. The control law is based on an outer-loop admittance control and an inner-loop full-pose geometric controller. Moreover, the interaction forces are estimated by a wrench observer. The effectiveness of the theoretical results has been also tested in real experiments.

Staub et al. (2018) proposed a design, called *OTHex*, tailored to the special case of cooperative beam manipulation. This design is similar to Ryll et al. (2017), where the AAUs are tilted of fixed angles to allow FA of the multirotor; this is important for cooperative manipulation as it allows the multirotor to resist lateral disturbances without the need for reorienting as in the coplanar case. The OTHex design also considers an AAU distribution less symmetric than Ryll et al. (2017), allowing a beam to pass through the propellers' volume.

The work by Morbidi et al. (2018) presents a platform design where the tilting of all propellers is synchronized so that all propellers tilt about the same radial and tangential angles. Their study can be applied for designs with active or passive tilting, thus $n_u = 6 + 2$. The authors determined a minimum-energy trajectory between two predefined boundary states; to achieve this goal an optimal control has been used by including also the dynamics of the brushless DC motors. Moreover, a deep analysis of the singularities of the allocation matrix has been presented. The tilting angles (α, β) come from a high-level tilt planner which is pre-computed offline and is known by the optimizer. In some sense, this work is the opposite of Rajappa et al. (2015) where optimal tilt angles were found to follow a pre-computed trajectory.

The two next works consider bidirectional AAUs. Rashad et al. (2017) proposed a design aimed at maximizing the actuation wrench while considering bidirectional AAUs. This leads to an OD design that has been validated in simulation with external wrench disturbances. The wrench maximization also results in only radial tilting. Their design was later demonstrated on a prototype with **APhI.1** capabilities in Rashad et al. (2019), however, with unidirectional propellers.

Myeong et al. (2019) also demonstrated a prototype hexarotor, with the propellers being placed in Y-formation. In their design, two of the motor pairs are placed along a horizontal shaft and can rotate independently in pairs, thus obtaining $n_u = 6 + 1$. The design is similar to a T-shaped trirotor with each shaft containing two propellers rotating in opposite to produce zero moment. The platform is endowed with a mechanism that allows it to apply a force on walls to aid in their inspection.

9. Heptarotor (seven AAUs)

This case is of particular interest because for designs that have AAUs with fixed orientation (i.e., $n_u = N$) and all unidirectional thrust propellers, the condition $N \geqslant 7$ is necessary to achieve OD as proven in Tognon and Franchi (2018) (see also Table 11). Despite its OA/OD ability with fixed AAUs, the design is not popular and only two examples of such designs have been found in the literature.

Arguably, heptarotor designs first appeared in Nikou et al. (2015), where an optimal design for a manipulation

Table 11 Recapitulative table for the heptarotors ($N = 7$)

Apparition	n_u	Properties	Abilities	Maturity	Figure
Nikou et al. (2015)	7	OA, FA	H.4, TT.4, APhI.3	Realistic simulation (TT.4)	Figure 26
Tognon and Franchi (2018)	7	OA, OD	H.4, TT.4, APhI.0	Realistic simulation (TT.4)	Figure 27

Table 12 Recapitulative table for the octorotors and the platforms with more than eight rotors $N \geqslant 8$

Apparition	n_u	DoFs	Properties	Abilities	Maturity	Figure
Romero et al. (2007)Fu et al. (2017)	8		OA, OD	H.4, TT.4, APhI.0	Prototype	Figure 29
Park et al. (2018)	8		OD	H.4, TT.4, APhI.0	Prototype	Figure 31
Brescianini and D'Andrea (2016)	8(Bi)		OA, OD	H.4, TT.4, APhI.0	Prototype	Figure 32
Allenspach et al. (2020)	12	$(\alpha_1, \alpha_2), (\alpha_3, \alpha_4), (\alpha_5, \alpha_6), (\alpha_7, \alpha_8), (\alpha_9, \alpha_10), (\alpha_11, \alpha_12)$	OA, OD	H.4, TT.4, APhI.0	Prototype	Figure 25

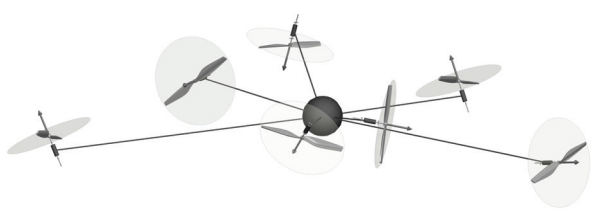

Fig. 26. Conceptual three-dimensional kinematic representation of the heptarotor design presented in Nikou et al. (2015).

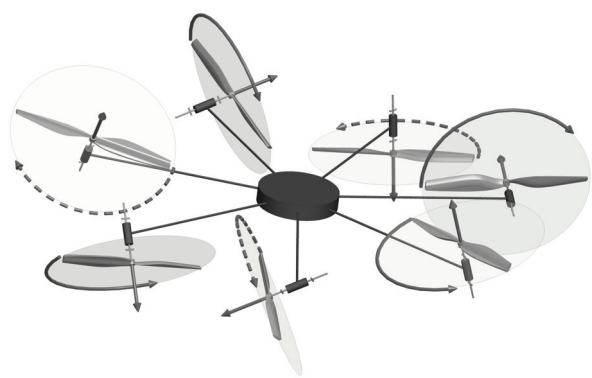

Fig. 27. Conceptual three-dimensional kinematic representation of the heptarotor design presented in Tognon and Franchi (2018).

task with body-fixed end-effector was considered, see Figure 26. The unidirectional AAUs constraint is considered explicitly. The optimization considers the condition number of $\boldsymbol{F}$ to ensure that the wrench produced is not sensitive to small deviations of the AAUs generated thrust. In addition, the aerodynamic interaction between the AAUs' airflow is considered, and sought to be minimized while keeping the total design volume reasonable. This design is evaluated in a simulation of trajectory tracking, in non-hovering orientation, subjected to disturbances and controlled via a backstepping approach.

The optimization design problem in Tognon and Franchi (2018) assumes fixed positions of the AAUs, radially around the CoM, and optimizes their respective tilting. A major design criterion considered was a minimum allocation-matrix condition number, which aims at an equal sharing of the effort needed to generate wrenches in any direction. In addition, the notion of "balanced design" was introduced which guarantees an equal sharing of the extra effort needed to keep all AAUs' individual thrust positive. An associated controller relying on model inversion and PID is proposed alongside. The general optimal design problem is proposed to make the design OD while minimizing the range of required control inputs to hover in any orientation. It is described and applied for $N = 7$, with an extensive realistic simulation of trajectory tracking, with several non-idealities described in the corresponding technical report. The authors hinted that minimizing the condition number of $\boldsymbol{F}$, $\kappa(\boldsymbol{F})$, for a balanced design, minimizes the norm of the input. The result of this optimization for $N = 7$ is shown in Figure 27. The $\mathfrak{F}_1$ set of this design is presented in Figure 28. A prototype of the platform was presented in Hamandi et al. (2020) to demonstrate the OD ability of the design.

10. Other designs with eight AAUs or more

We group all other platforms with $N \geqslant 8$ together, where we note that the majority of such designs consist of octorotors (Table 12). Some notable exceptions are the commercial "heavy lifter," which are coplanar/collinear multirotor designs. Examples include Aerones (2016) with $N = 14$, and *Volocopter*[6] *with* $N = 18$

The preference of the octorotor design over others in the literature can be explained by the favored symmetric

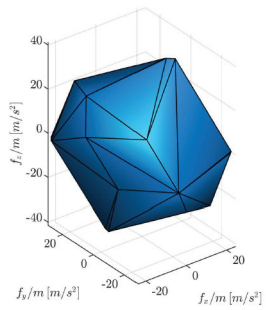

Fig. 28. Visualization of the $\mathfrak{F}_1$ set of the design presented in Tognon and Franchi (2018). The design consists of a heptarotor with fixed unidirectional propellers, with orientations designed to allow omnidirectional flight. Here $N = 7$ and $n_u = 7$. Profile description: irregular icositetrahedron contained inside a sphere in $\mathbb{R}^3$.

multirotor design with an even number of propellers. Moreover, due to the required compactness of commercial platforms, it becomes important for the design to have the fewest propellers for the given application. A larger number of propellers adds more weight to the platform and requires a larger platform to avoid aerodynamic interactions between adjacent AAUs, and thus is only used when additional thrust is required.

10.1 Enhanced quadrotor design

Octorotor designs in this section can be seen as an attempt to overcome the translational under-actuation of coplanar/collinear quadrotors, by adding four AAUs with thrust oriented in the non-actuated directions, similarly to the pentarotor in Albers et al. (2010).

Romero et al. (2007) proposed a multirotor design based on a quadrotor design with four additional smaller AAUs, orthogonal to the four main ones. A conceptual kinematic design is shown in Figure 29. The extra AAUs are devoted to controlling the lateral motion of the multirotor. It is interesting to note that the lateral smaller propellers produce an airflow that perturbs the induced wind speed in the main propellers increasing its lift. This term is compensated by a feedforward linearization of the aerodynamics interaction to obtain a full decoupling between the rotational and translational movements. The trajectory tracking problem is then solved by resorting to a mixture of a model-independent PD controller, coupled with a model-dependent compensation of the Coriolis and gyroscopic non-linear torques. The $\mathfrak{F}_1$ set of this design is presented in Figure 30.

In Fu et al. (2017), the AAUs are also tilted in the lateral plane but are located differently, reducing the cross-wind which improved the efficiency; this results again in an FA design.

10.2 Optimized octorotor designs

Following these basic octorotor designs, some more refined designs can be found in the literature.

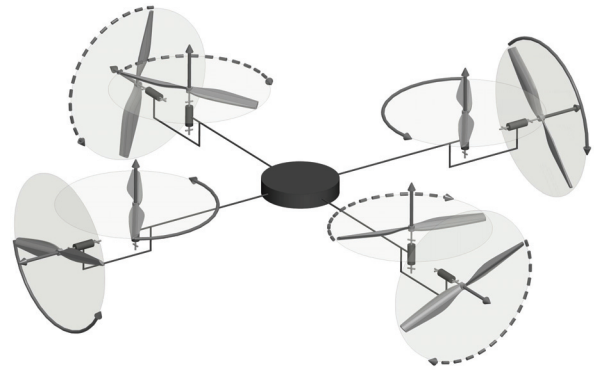

Fig. 29. Conceptual three-dimensional kinematic representation of the octorotor design presented in Romero et al. (2007).

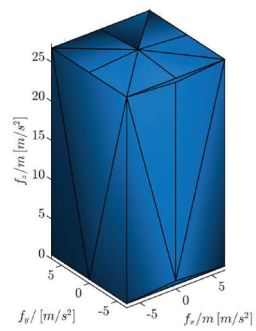

Fig. 30. Visualization of the $\mathfrak{F}_1$ set of the design presented in Romero et al. (2007); the $\mathfrak{F}_1$ set is normalized by the platform mass. The design consists of eight propellers, with four being collinear/coplanar with thrust pointing upwards to provide lift, and the other four pointing in the positive and negative x and y direction, respectively. Here $N = 8$ and $n_u = 8$. Profile description: cuboid with a square pyramid on top.

Park et al. (2016, 2018) included aerodynamic interferences in the optimization problem. The goal of the optimization is to find an optimal wrench generation and an optimal rotor location within a maximum allowable volume. The first design was presented in Park et al. (2016) with $N = 6$, and then a similar design was presented later in Park et al. (2018) with $N = 8$. The final design consists of a longitudinal bar along which propellers are placed in fixed non-symmetric positions as shown in Figure 31 showing the case with $N = 8$, with $n_u = N$. Eventually, a PID (system-independent) control strategy is implemented. In this case, to obtain bidirectional propulsion, two unidirectional propellers have been stacked together in opposite directions.

An optimized octorotor design with bidirectional propellers is presented in Brescianini and D'Andrea (2016) and shown in Figure 32. The platform is intended to be omnidirectional, and was designed by placing propellers on the edges of an octahedron to have a rotational invariant inertia tensor. Then the rotor disk orientations were chosen to maximize a measure of the platform's agility, i.e., the

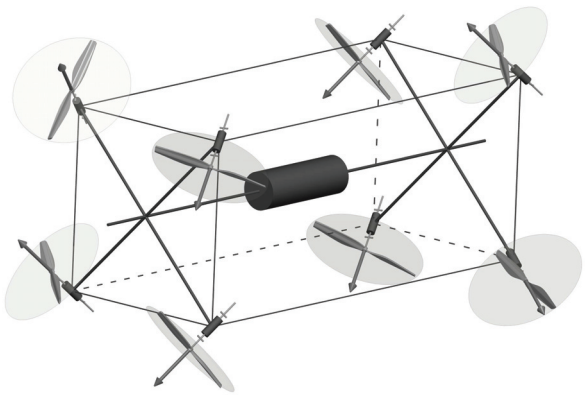

Fig. 31. Conceptual three-dimensional kinematic representation of the octorotor design presented in Park et al. (2016, 2018)..

norm of the maximum attainable force–torque in any direction. As the system is FA, the authors exploit the feedback linearization technique to derive the controller.

In the technical report attached to Tognon and Franchi (2018), which has been introduced in the previous section, an application for $N = 8$ unidirectional propellers is briefly introduced to show the generality of the described design method for fixed unidirectional AAUs.

Finally, Allenspach et al. (2020) presented a dodecacopter that is an upgrade of the *Voliro* design presented in Kamel et al. (2018), where the platform is endowed with 12 propellers, mounted on 6 equally spaced arms in pairs, where each of these pairs share the same spinning axis and rotate in opposing directions. Each arm of the platform can rotate about its radial axis, and thus $n_u = 12 + 6$. The platform is designed to provide position-omnidirectionality, in addition to force-omnidirectionality that is discussed in the paper. The design capabilities are demonstrated with a working prototype.

11. Discussion

Throughout the review, we have realized a few patterns in the presented designs, such as: (1) the focus on symmetrical designs; (2) the use of unidirectional propellers; (3) ignoring aerodynamic interaction between propellers; (4) and, finally, system modeling not considering actuation limits.

While these patterns are prevalent, there has been some attempts in the literature to break these renditions. However, the full analysis of each, the corresponding advantages, and their incorporation in future designs is still to be done.

11.1 Platform symmetry

We can see that in the presented literature, the majority of designs enforce some symmetry assumptions. These symmetries vary from placing all propellers on a horizontal axis; assuming the same tilt for all propellers (with varying directions); assuming all propellers to be placed on a circumference around the geometric center of the platform, or finally having an even number of propellers. The symmetry is usually done to simplify the mechanical design and the resulting modeling and control, which in turn results in stable platforms and easy to mass-produce designs. However, we have seen that Tognon and Franchi (2018) by optimizing the tilt of the propellers about the horizontal axis, independently of any symmetry between the tilts, was able to achieve OD with $N \geqslant 7$. Conversely, Brescianini and D'Andrea (2016) achieved OD with a design where the propellers are no longer placed on a horizontal axis, but

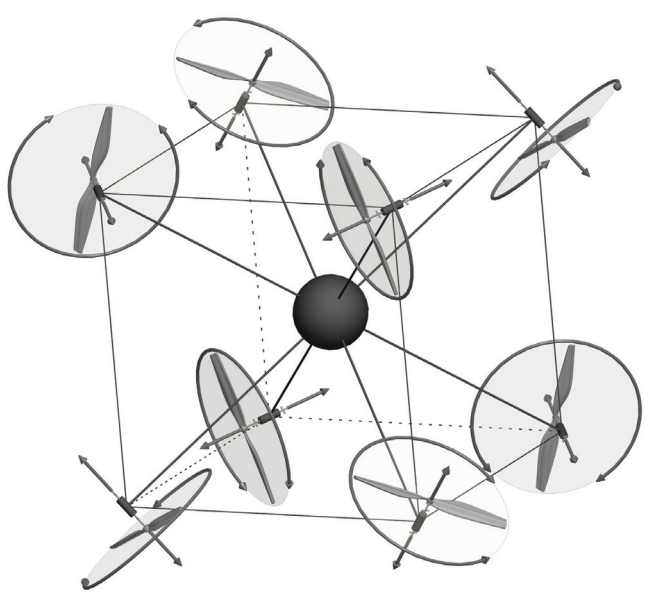

Fig. 32. Conceptual three-dimensional kinematic representation of the OD octorotor design presented in Brescianini and D'Andrea (2016).

rather on the vertices of an octahedron. Finally, Nikou et al. (2015) removed any symmetry assumption and optimized the location and orientation of all propellers for a given application. As such, we can see that the relaxation of symmetry heuristics, combined with an optimization of the platform based on performance metrics can achieve a wider allocation space, and advance multirotor designs beyond what is currently possible.

11.2 Bi-directional propellers

We realized throughout the review that the use of bidirectional propellers is scarce, where only a few of the cited designs (Brescianini and D'Andrea, 2016; De Martini et al., 2017; Park et al., 2016, 2018; Rashad et al., 2017) decided to use such propellers, in spite of the benefit of controlling the thrust produced by the propeller in both directions. One possible motivation is the "singular" behavior near the zero-thrust region (Park et al., 2018), where the propeller tends to take longer to reverse their direction of rotation (Brescianini and D'Andrea, 2016). Moreover, commercial solutions for reversible electronic speed control are scarce and the geometry of the propeller is less energy efficient than the unidirectional counterpart. Lastly, at low speed, the controllability of the exerted forces is very low, thus difficult to be used in practice. The variable pitch propeller can mitigate some of these issues but they come at the expense of additional mechanical complexity and weight, which is also not very practical. Another solution that can be achieved in this part is the use of bidirectional propellers while avoiding the allocation near the inversion zone of each propeller. However, proper optimization algorithms must be designed for this regards, in addition to the need for a redundancy resolution in the allocation capabilities.

11.3 Aerodynamic interaction between propellers

The field at large could benefit from further studies on the aerodynamic effects at play, especially the interplay between AAUs cross-wind. The integration of the aerodynamic effects in the model used for control synthesis should permit feed-forward cancellation of these effects. This is of particular importance for the development of platforms endowed with fine force interaction capabilities. In addition, a good model of the aerodynamic effects could be leveraged in the design process, extending Nikou et al. (2015) and Park et al. (2018), or benefiting from the work of Waslander and Wang (2009).

11.4 Actuator limits

Actuator saturation is often dismissed in theoretical studies but plays an important role in practice. Indeed, saturations hinder the multirotor dynamics, and if not taken into account properly, can result in destabilizing the control actions, in particular in dynamical maneuvers or while in physical interaction. While a few papers study the saturation's effect on control (Franchi et al., 2018; Invernizzi and Lovera, 2017), we found only one work that incorporates the actuation limits in their design Jiang et al. (2017). In particular, Jiang et al. (2017) optimized propeller tilt angles of a tilted hexarotor (similar to Figure 21, top) to increase the possible platform lift while increasing the efficiency of the platform.

12. Conclusion

In this literature review of multirotor design, we first proposed a universal parametrization of multirotors in order to try to homogenize the vast literature on the topic. Based on this parametrization we first proposed a set of system properties and system capabilities for multirotors. Then we evaluated the vast literature on multirotor design and highlighted key conditions to reach certain properties. Finally, we grouped the reviewed designs into classes based on their number of AAUs as we found it more natural for the readers, and showed how designs from each class expanded the allocation capabilities of such class. To the best of the authors' knowledge, this literature review is the first of its kind, and encompasses most of the relevant designs on the topic.

From this literature review and the proposed taxonomy, we could see that initial designs started as a method to upgrade a classical helicopter aircraft (i.e., a birotor, with one variable pitch main rotor with a cyclic input on one axis, and one perpendicular in the tail), then either the design degenerated the platform to push the aerodynamics of the design to have flight with the fewest controls, or increased the number of actuators and changed their disposition about the CoM of the platform to achieve more stable platforms (quadrotors), or achieve higher levels of actuation (MDT, FA, OA, OD). Eventually, coplanar/collinear quadrotors became the base case for most designs thanks to their availability, stability, and the simplicity of their mechanical design.

The changes from classical designs entailed advantages in allocation and allowed the platforms to be able to interact with the environment, resist disturbances, apply lateral forces without a change in direction, and become robust to AAU failures. In our summary of each platform, we showed how each design corresponded to a specific set of abilities and properties. Recent platform designs started shifting more towards achieving omnidirectional flights, or decoupled force-moment allocation, preferred for physical aerial manipulation tasks, with this last application increasing in popularity thanks to the technological impact it entails.

Funding

The author(s) disclosed receipt of the following financial support for the research, authorship, and/or publication of this article: This work has been partially funded by the European Commission (project H2020 AERIAL-CORE; EC 871479).

ORCID iDs

Mahmoud Hamandi https://orcid.org/0000-0001-9149-3741
Quentin Sable https://orcid.org/0000-0001-9153-7927
Marco Tognon https://orcid.org/0000-0003-1700-9637
Antonio Franchi https://orcid.org/0000-0002-5670-1282

Notes

1. Here $\mathbb{S}^n = \{\boldsymbol{x} \in \mathbb{R}^{n+1} | \boldsymbol{x} = 1\}$.
2. Here $SO(3) = \{\mathrm{R} \in \mathbb{R}^{3\times 3} | \mathrm{R}^{\mathrm{T}}\mathrm{R} = \boldsymbol{I}_3, \det(\mathrm{R}) = 1\}$, where $\boldsymbol{I}_i \in \mathbb{R}^{i\times i}$ is the identity matrix of dimension i.
3. We refer to f_x, f_y and f_z as the respective components of $\boldsymbol{f}$ along $\boldsymbol{x}_B$, $\boldsymbol{y}_B$, and $\boldsymbol{z}_B$.
4. Here $\mathrm{ball}_{\mathbb{R}^3}(R)$ for a certain $R \in \mathbb{R}_{>0}$ is defined such that given a vector $\boldsymbol{x} \in \mathbb{R}^3$, $\boldsymbol{x} \in \mathrm{ball}_{\mathbb{R}^3}(R)$ if $||\boldsymbol{x}|| \leqslant R$.
5. See http://skybornetech.com/
6. See http://www.volocopter.com.

References

Aerones (2016) Heavy duty drone for high paylaod transportation. https://www.aerones.com/ (accessed 31 August 2020).

Albers A, Trautmann S, Howard T, Nguyen T, Frietsch M and Sauter C (2010) Semi-autonomous flying robot for physical interaction with environment. In: *2010 IEEE Conference on Robotics, Automation and Mechatronics*, pp. 441–446.

Allenspach M, Bodie K, Brunner M, et al. (2020) Design and optimal control of a tiltrotor micro-aerial vehicle for efficient omnidirectional flight. *The International Journal of Robotics Research* 39(10–11): 1305–1325.

Amiri N, Ramirez-Serrano A and Davies R (2011) Modelling of opposed lateral and longitudinal tilting dual-fan unmanned aerial vehicle. *IFAC Proceedings Volumes* 44(1): 2054–2059.

Anzai T, Zhao M, Chen X, et al. (2017) Multilinked multirotor with internal communication system for multiple objects transportation based on form optimization method. In: *2017 IEEE/RSJ International Conference on Intelligent Robots and Systems*, Vancouver, BC, Canada, pp. 5977–5984.

Badr S, Mehrez O and Kabeel A (2016) A novel modification for a quadrotor design. In: *2016 International Conference on Unmanned Aircraft Systems*, Arlington, VA, USA, pp. 702–710.

Barber C, Dobkin D and Huhdanpaa H (1996) The quickhull algorithm for convex hulls. *ACM Transactions on Mathematical Software* 22(4): 469–483.

Bicego D (2019) *Design and Control of Multi-Directional Thrust Multi-Rotor Aerial Vehicles With Applications to Aerial Physical Interaction Tasks*. Ph.D. thesis, Université de Toulouse.

Blouin C and Lanteigne E (2014) Pitch control of an oblique active tilting bi-rotor. In: *2014 International Conference on Unmanned Aircraft Systems*, Orlando, FL, USA, pp. 791–799.

Bouabdallah S, Noth A and Siegwart R (2004) PID vs LQ control techniques applied to an indoor micro quadrotor. In: *2004 IEEE/RSJ International Conference on Intelligent Robots and Systems*, Sendai, Japan, pp. 2451–2456.

Bouabdallah S and Siegwart R (2005) Backstepping and sliding-mode techniques applied to an indoor micro quadrotor. In: *2005 IEEE International Conference on Robotics and Automation*, Barcelona, Spain, pp. 2247–2252.

Brescianini D and D'Andrea R (2016) Design, modeling and control of an omni-directional aerial vehicle. In: *2016 IEEE International Conference on Robotics and Automation*, Stockholm, Sweden, pp. 3261–3266.

Bronz M, Smeur E, Garcia de Marina H and Hattenberger G (2017) Development of a fixed-wing mini UAV with transitioning flight capability. In: *35th AIAA Applied Aerodynamics Conference*.

Byrd RH, Gilbert JC and Nocedal J (2000) A trust region method based on interior point techniques for nonlinear programming. *Mathematical programming* 89(1): 149–185.

Cardoso D, Raffo G and Esteban S (2016) A robust adaptive mixing control for improved forward flight of a tilt-rotor UAV. In: *2016 IEEE 19th International Conference on Intelligent Transportation Systems (ITSC)*, Rio de Janeiro, Brazil, pp. 1432–1437.

Chowdhury A, Kulhare A and Raina G (2012) A generalized control method for a tilt-rotor uav stabilization. In: *2012 IEEE International Conference on Cyber Technology in Automation, Control, and Intelligent Systems (CYBER)*, Bangkok, Thailand, pp. 309–314.

Crowther B, Lanzon A, Maya-Gonzalez M and Langkamp D (2011) Kinematic analysis and control design for a nonplanar multirotor vehicle. *Journal of Guidance, Control, and Dynamics* 34(4): 1157–1171.

De Martini D, Gramazio G, Bertini A, Rottenbacher C and Facchinetti T (2017) Design and modeling of a quadcopter with double axis tilting rotors. *Unmanned Systems* 5(3): 169–180.

Devlin T, Dickerhoff R, Durney K, et al. (2018) Elbowquad: Thrust vectoring quadcopter. In: *2018 AIAA Information Systems-AIAA Infotech@ Aerospace*, p. 0893.

Donadel R, Raffo G and Becker L (2014) Modeling and control of a tiltrotor UAV for path tracking. *IFAC Proceedings Volumes* 47(3): 3839–3844.

Elkhatib O (2017) *Control Allocation of a Tilting Rotor Hexacopter*. B.S. thesis, ETH Zurich

Escareno J, Sanchez A, Garcia O and Lozano R (2008) Triple tilting rotor mini-UAV: Modeling and embedded control of the attitude. In: *2008 American Control Conference*, Seattle, WA, USA, pp. 3476–3481.

Falanga D, Mueggler E, Faessler M and Scaramuzza D (2017) Aggressive quadrotor flight through narrow gaps with onboard sensing and computing using active vision. In: *2017 IEEE International Conference on Robotics and Automation*, Marina Bay Sands, Singapore, pp. 5774–5781.

Falconi R and Melchiorri C (2012) Dynamic model and control of an over-actuated quadrotor UAV. *IFAC Proceedings Volumes* 45(22): 192–197.

Franchi A, Carli R, Bicego D and Ryll M (2018) Full-pose tracking control for aerial robotic systems with laterally-bounded input force. *IEEE Transactions on Robotics* 34(2): 534–541.

Fu Z, Yang BXJ, Wu C and Wei Y (2017) Modeling and control of a new multicopter. In: *2017 36th Chinese Control Conference (CCC)*, Liaoning, China, pp. 6495–6500.

Genov B (2015) *The Convex Hull Problem in Practice: Improving the Running Time of the Double Description Method*. Dissertation, Universität Bremen.

Giribet J, Sanchez-Pena R and Ghersin A (2016) Analysis and design of a tilted rotor hexacopter for fault tolerance. *IEEE Transactions on Aerospace and Electronic Systems* 52(4): 1555–1567.

Gress G (2002) Using dual propellers as gyroscopes for tilt-prop hover control. In: *2002 Biennial International Powered Lift Conference and Exhibit*, p. 5968.

Hamandi M, Sawant K, Tognon M and Franchi A (2020) Omni-plus-seven (O7 +): An omnidirectional aerial prototype with a minimal number of unidirectional thrusters. In: *2020 International Conference on Unmanned Aircraft Systems*, pp. 754–761.

Haus T, Orsag M and Bogdan S (2016) Design considerations for a large quadrotor with moving mass control. In: *2016 International Conference on Unmanned Aircraft Systems*, Arlington, VA, USA, pp. 1327–1334.

Haus T, Orsag M and Bogdan S (2017) A concept of a non-tilting multirotor-UAV based on moving mass control. In: *2017 International Conference on Unmanned Aircraft Systems*, Miami, FL, USA, pp. 1618–1624.

Hua M, Hamel T, Morin P and Samson C (2015) Control of vtol vehicles with thrust-tilting augmentation. *Automatica* 52: 1–7.

Invernizzi D and Lovera M (2017) Geometric tracking control of a quadcopter tiltrotor UAV. *IFAC-PapersOnLine* 50(1): 11565–11570.

Jiang G and Voyles R (2014) A nonparallel hexrotor uav with faster response to disturbances for precision position keeping. In: *2014 IEEE International Symposium on Safety, Security and Rescue Robotics*, Toyako-cho, Hokkaido, Japan, pp. 1–5.

Jiang G, Voyles R, Sebesta K and Greiner H (2017) Estimation and optimization of fully-actuated multirotor platform with nonparallel actuation mechanism. In: *2017 IEEE/RSJ International Conference on Intelligent Robots and Systems (IROS)*. IEEE, pp. 6843–6848.

Kamel M, Verling S, Elkhatib O, et al. (2018) The Voliro omniorientational hexacopter: An agile and maneuverable tiltable-rotor aerial vehicle. *IEEE Robotics and Automation Magazine* 25(4): 34–44.

Kastelan D, Konz M and Rudolph J (2015) Fully actuated tricopter with pilot-supporting control. *IFAC-PapersOnLine* 48(9): 79–84.

Kataoka Y, Sekiguchi K and Sampei M (2011) Nonlinear control and model analysis of trirotor UAV model. *IFAC Proceedings Volumes* 44(1): 10391–10396.

Kawasaki K, Motegi Y, Zhao M, Okada K and Inaba M (2015) Dual connected bi-copter with new wall trace locomotion feasibility that can fly at arbitrary tilt angle. In: *2015 IEEE/RSJ International Conference on Intelligent Robots and Systems*, Hamburg, Germany, pp. 524–531.

Kendoul F, Fantoni I and Lozano R (2006) Modeling and control of a small autonomous aircraft having two tilting rotors. *IEEE Transactions on Robotics* 22(6): 1297–1302.

Festo AG & Co. KG (2016) Freemotionhandling. https://www.festo.com/net/SupportPortal/Files/443122/50017_Brosch_FreeMotionHandling_en_160329_lo_ES.pdf. (accessed 11 July 2018).

Khoo S, Norton M, Kumar J, et al. (2017) Robust control of novel thrust vectored 3D printed multicopter. In: *2017 36th Chinese Control Conference (CCC)*, Liaoning, China, pp. 1270–1275.

Kleder M (2020) CON2VERT - constraints to vertices. Matlab Central File Exchange. https://www.mathworks.com/matlabcentral/fileexchange/7894-con2vert-constraints-to-vertices (accessed 5 June 2021).

Long Y, Gelardos A and Cappelleri D (2014) A novel micro aerial vehicle design: The evolution of the omnicopter MAV. In: *ASME 2014 International Design Engineering Technical Conferences and Computers and Information in Engineering Conference*, Buffalo, NY, USA, V05AT08A092.

Long Y, Lyttle S, Pagano N and Cappelleri D (2012) Design and quaternion-based attitude control of the omnicopter mav using feedback linearization. In: *ASME International Design Engineering Technical Conference (IDETC)*, Chicago, IL, USA, pp. 1413–1421.

Mahony R, Kumar V and Corke P (2012) Multirotor aerial vehicles: Modeling, estimation, and control of quadrotor. *IEEE Robotics and Automation Magazine* 19(3): 20–32.

McArthur D, Chowdhury A and Cappelleri D (2017) Design of the i-Boomcopter UAV for environmental interaction. In: *2017 IEEE International Conference on Robotics and Automation*, Singapore, pp. 5209–5214.

Mehmood H, Nakamura T and Johnson E (2016) A maneuverability analysis of a novel hexarotor UAV concept. In: *2016 International Conference on Unmanned Aircraft Systems*, Arlington, VA, USA, pp. 437–446.

Michieletto G, Ryll M and Franchi A (2017) Control of statically hoverable multi-rotor aerial vehicles and application to rotor-failure robustness for hexarotors. In: *2017 IEEE International Conference on Robotics and Automation*, Singapore, pp. 2747–2752.

Michieletto G, Ryll M and Franchi A (2018) Fundamental actuation properties of multi-rotors: Force-moment decoupling and fail-safe robustness. *IEEE Transactions on Robotics* 34(3): 702–715.

Michini B, Redding J, Ure NK, Cutler M and How JP (2011) Design and flight testing of an autonomous variable-pitch quadrotor. In: *2011 IEEE International Conference on Robotics and Automation*, Shanghai, China, pp. 2978–2979.

Mistler V, Benallegue A and M'Sirdi NK (2001) Exact linearization and noninteracting control of a 4 rotors helicopter via dynamic feedback. In: *10th IEEE International Symposium on Robots and Human Interactive Communications*, Bordeaux, Paris, France, pp. 586–593.

Mohamed M and Lanzon A (2012) Design and control of novel tri-rotor UAV. In: *2012 UKACC International Conference on control (CONTROL)*, Cardiff, UK, pp. 304–309.

Morbidi F, Bicego D, Ryll M and Franchi A (2018) Energy-efficient trajectory generation for a hexarotor with dual-tilting propellers. In: *2018 IEEE/RSJ International Conference on Intelligent Robots and Systems*, Madrid, Spain, pp. 6226–6232.

Myeong W, Jung S, Yu B, Chris T, Song S and Myung H (2019) Development of wall-climbing unmanned aerial vehicle system for micro-inspection of bridges. In: *2019 IEEE International Conference on Robotics and Automation*, Montreal, Canada.

Nemati A and Kumar M (2014) Modeling and control of a single axis tilting quadcopter. In: *2014 American Control Conference*, Portland, OR, USA, pp. 3077–3082.

Nemati A, Soni N, Sarim M and Kumar M (2016) Design, fabrication and control of a tilt rotor quadcopter. In: *2016 ASME Dynamic Systems and Control Conference*. Minneapolis, MN, USA. American Society of Mechanical Engineers, V002T29A005.

Nikou A, Gavridis G and Kyriakopoulos K (2015) Mechanical design, modelling and control of a novel aerial manipulator. In: *2015 IEEE International Conference on Robotics and Automation*, Seattle, WA, USA, pp. 4698–4703.

Odelga M, Stegagno P and Bülthoff H (2016) A fully actuated quadrotor UAV with a propeller tilting mechanism: Modeling and control. In: *2016 IEEE/ASME International Conference*

on Advanced Intelligent Mechatronics, Banff, Alberta, Canada, pp. 306–311.

Oosedo A, Abiko S, Narasaki S, Kuno A, Konno A and Uchiyama M (2016) Large attitude change flight of a quad tilt rotor unmanned aerial vehicle. *Advanced Robotics* 30(5): 326–337.

Oung R, Bourgault F, Donovan M and D'Andrea R (2010) The distributed flight array. In: *2010 IEEE International Conference on Robotics and Automation*, Anchorage, AK, USA, pp. 601–607.

Papachristos C, Alexis K and Tzes A (2011) Design and experimental attitude control of an unmanned tilt-rotor aerial vehicle. In: *2011 International Conference on Robotics*, Tallinn, Estonia, pp. 465–470.

Papachristos C, Alexis K and Tzes A (2014) Efficient force exertion for aerial robotic manipulation: Exploiting the thrust-vectoring authority of a tri-tiltrotor UAV. In: *2014 IEEE International Conference on Robotics and Automation*, Hong Kong, China, pp. 4500–4505.

Papachristos C, Alexis K and Tzes A (2016) Dual-authority thrust-vectoring of a tri-tiltrotor employing model predictive control. *Journal of Intelligent and Robotic Systems* 81(3–4): 471.

Papachristos C and Tzes A (2013) Large object pushing via a direct longitudinally-actuated unmanned tri-tiltrotor. In: *2013 Mediterranean Conference on Control and Automation*, Crete, Greece, pp. 173–178.

Park S, Her J, Kim J and Lee D (2016) Design, modeling and control of omni-directional aerial robot. In: *2016 IEEE/RSJ International Conference on Intelligent Robots and Systems*, Daejeon, Korea, pp. 1570–1575.

Park S, Lee J, Ahn J, et al. (2018) Odar: Aerial manipulation platform enabling omni-directional wrench generation. *IEEE/ASME Transactions on Mechatronics* 23(4): 1907–1918.

Pose C, Giribet J and Ghersin A (2017) Hexacopter fault tolerant actuator allocation analysis for optimal thrust. In: *2017 International Conference on Unmanned Aircraft Systems*, Miami, FL, USA, pp. 663–671.

Pounds P, Mahony R and Corke P (2010) Modelling and control of a large quadrotor robot. *Control Engineering Practice* 18(7): 691–699.

Pounds P, Mahony R, Hynes P and Roberts JM (2002) Design of a four-rotor aerial robot. In: *Proceedings of the 2002 Australasian Conference on Robotics and Automation (ACRA 2002)*. Australian Robotics & Automation Association, pp. 145–150.

Prothin S and Moschetta JM (2013) A vectoring thrust coaxial rotor for micro air vehicle: Modeling, design and analysis. In: *ERCOFTAC International Symposium 'Unsteady separation in fluid-structure'*, Mykonos, Greece.

Rajappa S, Ryll M, Bülthoff H and Franchi A (2015) Modeling, control and design optimization for a fully-actuated hexarotor aerial vehicle with tilted propellers. In: *2015 IEEE International Conference on Robotics and Automation*, Seattle, WA, USA, pp. 4006–4013.

Ramp M and Papadopoulos E (2015) On modeling and control of a holonomic vectoring tricopter. In: *2015 IEEE/RSJ International Conference on Intelligent Robots and Systems*, Hamburg, Germany, pp. 662–668.

Rashad R, Engelen J and Stramigioli S (2019) Energy tank-based wrench/impedance control of a fully-actuated hexarotor: A geometric port-hamiltonian approach. In: *2019 IEEE International Conference on Robotics and Automation*, Montreal, Canada, pp. 6418–6424.

Rashad R, Kuipers P, Engelen J and Stramigioli S (2017) Design, modeling, and geometric control on SE(3) of a fully-actuated hexarotor for aerial interaction. *arXiv preprint arXiv:1709.05398*.

Romero H, Salazar S, Sanchez A and Lozano R (2007) A new UAV configuration having eight rotors: Dynamical model and real-time control. In: *2007 46th IEEE Conference on Decision and Control*, New Orleans, LA, USA, pp. 6418–6423.

Rongier P, Lavarec E and Pierrot F (2005) Kinematic and dynamic modeling and control of a 3-rotor aircraft. In: *2005 IEEE International Conference on Robotics and Automation*, Barcelona, Spain, pp. 2606–2611.

Ryll M, Bicego D and Franchi A (2016) Modeling and control of FAST-Hex: a fully-actuated by synchronized-tilting hexarotor. In: *2016 IEEE/RSJ International Conference on Intelligent Robots and Systems*, Daejeon, South Korea, pp. 1689–1694.

Ryll M, Bülthoff H and Giordano P (2012) Modeling and control of a quadrotor uav with tilting propellers. In: *2012 IEEE International Conference on Robotics and Automation*, Paul, MN, USA, pp. 4606–4613.

Ryll M, Bülthoff H and Giordano P (2013) First flight tests for a quadrotor uav with tilting propellers. In: *2013 IEEE International Conference on Robotics and Automation*, Karlsruhe, Germany, pp. 295–302.

Ryll M, Bülthoff H and Giordano P (2015) A novel overactuated quadrotor unmanned aerial vehicle: Modeling, control, and experimental validation. *IEEE Transactions on Control Systems Technology* 23(2): 540–556.

Ryll M, Muscio G, Pierri F, et al. (2017) 6D physical interaction with a fully actuated aerial robot. In: *2017 IEEE International Conference on Robotics and Automation*, Singapore, pp. 5190–5195.

Soto-Guerrero D and Ramírez-Torres JG (2018) The hexapodopter: A hybrid flying hexapod—holonomic flying analysis. *Journal of Mechanisms and Robotics* 10(5): 051008 .

Saeed A, Younes A, Islam S, Dias J, Seneviratne L and Cai G (2015) A review on the platform design, dynamic modeling and control of hybrid UAVs. In: *2015 International Conference on Unmanned Aircraft Systems*, Denver, CO, USA, pp. 806–815.

Salazar-Cruz S and Lozano R (2005) Stabilization and nonlinear control for a novel trirotor mini-aircraft. In: *2005 IEEE International Conference on Robotics and Automation*, Barcelona, Spain, pp. 2612–2617.

Salazar-Cruz S, Lozano R and Escareño J (2009) Stabilization and nonlinear control for a novel trirotor mini-aircraft. *Control Engineering Practice* 17(8): 886–894.

Sanchez A, Escareno J, Garcia O and Lozano R (2008) Autonomous hovering of a noncyclic tiltrotor UAV: Modeling, control and implementation. *IFAC Proceedings Volumes* 41(2): 803–808.

Sarkisov Y, Kim MJ, Bicego D, et al. (2019) Development of SAM: Cable-suspended aerial manipulator. In: *2019 IEEE International Conference on Robotics and Automation*, Montreal, Canada.

Scholz G, Popp M, Ruppelt J and Trommer G (2016) Model independent control of a quadrotor with tiltable rotors. In: *2016 IEEE/ION Position, Location and Navigation Symposium (PLANS)*, Savannah, GA, USA, pp. 747–756.

Segui-Gasco P, Al-Rihani Y, Shin H and Savvaris A (2014) A novel actuation concept for a multi rotor UAV. *Journal of Intelligent and Robotics Systems* 74(1–2): 173–191.

Şenkul F and Altuğ E (2013) Modeling and control of a novel tilt–roll rotor quadrotor UAV. In: *2013 International Conference on Unmanned Aircraft Systems*, Atlanta, GA, USA, pp. 1071–1076.

Şenkul F and Altuğ E (2014) Adaptive control of a tilt-roll rotor quadrotor UAV. In: *2014 International Conference on Unmanned Aircraft Systems*, Orlando, FL, USA, pp. 1132–1137.

Servais É, D'Andrea-Novel B and Mounier H (2015a) Ground control of a hybrid tricopter. In: *2015 International Conference on Unmanned Aircraft Systems*, Denver, CO, USA, pp. 945–950.

Servais É, Mounier H and D'Andrea-Novel B (2015b) Trajectory tracking of trirotor UAV with pendulum load. In: *2015 20th International Conference on Methods and Models in Automation and Robotics (MMAR)*, Międzyzdroje, Poland, pp. 517–522.

Staub N, Bicego D, Sablé Q, Arellano-Quintana V, Mishra S and Franchi A (2018) Towards a flying assistant paradigm: The OTHex. In: *2018 IEEE International Conference on Robotics and Automation*, Brisbane, Australia, pp. 6997–7002.

Tadokoro Y, Ibuki T and Sampei M (2017) Maneuverability analysis of a fully-actuated hexrotor UAV considering tilt angles and arrangement of rotors. *IFAC-PapersOnLine* 50(1): 8981–8986.

Tognon M and Franchi A (2018) Omnidirectional aerial vehicles with unidirectional thrusters: Theory, optimal design, and control. *IEEE Robotics and Automation Letters* 3(3): 2277–2282.

Waslander S and Wang C (2009) Wind disturbance estimation and rejection for quadrotor position control. In: *AIAA Infotech@Aerospace Conference and AIAA Unmanned... Unlimited conference*, p. 1983.

Yih C (2016) Flight control of a tilt-rotor quadcopter via sliding mode. In: *2016 International Automatic Control Conference (CACS)*, Taichung, Taiwan, pp. 65–70.

Yoon S, Lee S, Lee B, Kim C, Lee Y and Sung S (2013) Design and flight test of a small tri-rotor unmanned vehicle with a lqr based onboard attitude control system. *International Journal of Innovative Computing, Information and Control* 9(6): 2347–2360.

Yoshikawa T (1985) Manipulability of robotic mechanisms. *The International Journal of Robotics Research* 4(2): 3–9.

Young WR (1982) *The Helicopters: The Epic of Flight*. Time-Life Books.

Zhang W, Mueller M and D'Andrea R (2016) A controllable flying vehicle with a single moving part. In: *2016 IEEE International Conference on Robotics and Automation*, Stockholm, Sweden, pp. 3275–3281.

Zhao M, Kawasaki K, Chen X and Noda S (2017) Whole-body aerial manipulation by transformable multirotor with two-dimensional multilinks. In: *2017 IEEE International Conference on Robotics and Automation*, Singapore, pp. 5175–5182.